

1 **Short title:** Control of mRNA translation by *cis*-NATs

2

3 Control of cognate sense mRNA translation by *cis*-natural antisense RNAs

4

5 Jules Deforges¹, Rodrigo S Reis¹, Philippe Jacquet¹, Shaoline Sheppard¹, Veerendra P. Gadekar²,
6 Gene Hart-Smith³, Andrea Tanzer², Ivo L Hofacker², Christian Iseli⁴, Ioannis Xenarios⁴, Yves
7 Poirier¹

8

9 ¹Department of Plant Molecular Biology, University of Lausanne, Biophore Building, CH-1015
10 Lausanne, Switzerland

11 ²Institute of Theoretical Chemistry, University of Vienna, Währinger Str 17, A-1090 Vienna,
12 Austria

13 ³ School of Biotechnology and Biomolecular Sciences, University of New South Wales, Sydney,
14 Australia

15 ⁴Swiss Institute of Bioinformatics, Lausanne CH-1015, Switzerland

16

17 **Footnotes:**

18 **Author Contributions**

19 JD, RSR and YP conceived and designed the study. JD performed all experiments except for the
20 establishment and performance of the protoplast transformation assay done by RSR. Bioinformatic
21 analysis of the data was performed by JD and PJ, whereas proteomic analysis was performed by
22 GHS. Analysis of the coding potential of *cis*-NATs was done by VPG, AT and ILH, whereas
23 analysis of *cis*-NATs:sense mRNA configuration and main characteristics was done by SP and JD.
24 Bioinformatic support was also provided by CI and IX. JD, RSR and YP wrote the paper. All
25 authors read and approved the final manuscript. YP agrees to serve as the author responsible for
26 contact and ensures communication.

27

28 This work was supported by a Sinergia grant (CRSII3_154471) from the Swiss National Fund to
29 YP and ILH. The Swiss Institute of Bioinformatic (SIB) and Vital-IT Center for high-performance
30 computing of the SIB are supported by University of Lausanne and the Swiss Federal Government.

31

32 Corresponding author: yves.poirier@unil.ch

33

34 **One-sentence summary:** A robust pipeline identifies and experimentally validates *cis*-natural
35 antisense transcripts controlling cognate sense mRNA translation.

37 **Abstract**

38 *Cis*-Natural Antisense Transcripts (*cis*-NATs), which overlap protein coding genes and are
39 transcribed from the opposite DNA strand, constitute an important group of non-coding RNAs.
40 Whereas several examples of *cis*-NATs regulating the expression of their cognate sense gene are
41 known, most *cis*-NATs function by altering the steady-state level or structure of mRNA via changes
42 in transcription, mRNA stability or splicing, and very few cases involve the regulation of sense
43 mRNA translation. This study was designed to systematically search for *cis*-NATs influencing
44 cognate sense mRNA translation in *Arabidopsis thaliana*. Establishment of a pipeline relying on
45 sequencing of total polyA⁺ and polysomal RNA from *Arabidopsis* grown under various conditions
46 (i.e., nutrient deprivation and phytohormone treatments) allowed the identification of 14 *cis*-NATs
47 whose expression correlated either positively or negatively with cognate sense mRNA translation.
48 Using a combination of *cis*-NAT stable over-expression in transgenic plants and transient
49 expression in protoplasts, the impact of *cis*-NAT expression on mRNA translation was confirmed
50 for 4 out of 5 tested *cis*-NAT:sense mRNA pairs. These results expand the number of *cis*-NATs
51 known to regulate cognate sense mRNA translation and provide a foundation for future studies of
52 their mode of action. Moreover, this study highlights the role of this class of non-coding RNAs in
53 translation regulation.

54

55

56

58 **Introduction**

59 A large proportion of the genome of eukaryotes is transcribed into RNA that is not coding for
60 proteins or house-keeping RNAs (e.g. tRNAs, ribosomal RNAs) (Djebali et al., 2012). Whereas
61 first being considered as transcriptional noise, non-coding RNAs have emerged as major regulators
62 of gene expression (Rinn and Chang, 2012; Bonasio and Shiekhattar, 2014; Chekanova, 2015;
63 Ransohoff et al., 2018). Besides the well-characterized small RNAs that include short interfering
64 RNAs (siRNAs) and micro RNAs (miRNAs), abundant long non-coding RNAs (lncRNAs) have
65 been identified across a wide spectrum of organisms. LncRNAs are typically defined as capped and
66 polyadenylated transcripts longer than 200 bases that do not contain conserved open reading frame
67 capable of encoding proteins (Rinn and Chang, 2012; Bonasio and Shiekhattar, 2014; Chekanova,
68 2015; Ransohoff et al., 2018). However, recent studies have indicated that some lncRNAs could
69 associate with ribosomes and, in some cases, generate small peptides (Ji et al., 2015; Hsu et al.,
70 2016; Bazin et al., 2017). Whereas most of the lncRNAs identified by genome-wide studies have
71 yet unknown functions, an increasing number has been shown to be involved in critical biological
72 processes such as X chromosome inactivation in mammals (Brockdorff et al., 1992) or flowering in
73 plants (Liu et al., 2010; Heo and Sung, 2011).

74

75 LncRNAs located in intergenic regions relative to coding genes are defined as long intergenic non-
76 coding RNA (lincRNAs), whereas lncRNAs overlapping coding genes and transcribed from the
77 opposite DNA strand are categorized as *cis*-Natural Antisense Transcripts (*cis*-NATs) (Rinn and
78 Chang, 2012). In addition, lincRNAs able to bind target mRNAs by partial base-pair
79 complementarity are defined as *trans*-Natural Antisense Transcripts (*trans*-NAT) (Lapidot and
80 Pilpel, 2006). *Cis*-NATs are widespread in eukaryotes, with 20–70% of coding genes having an
81 associated *cis*-NAT in *Saccharomyces cerevisiae*, *Drosophila melanogaster*, mice, human, and
82 *Arabidopsis thaliana* (Faghihi and Wahlestedt, 2009; Liu et al., 2015). *Cis*-NATs can overlap
83 completely with their cognate mRNAs or only at the 5' (head-to-head orientation) or the 3' end (tail-
84 to-tail orientation).

85

86 Whereas various modes of action have been reported for lncRNAs impacting the regulation of
87 target gene expression, the majority involves changes in the steady-state level or structure of mRNA
88 via changes in transcription, mRNA stability or splicing (Rinn and Chang, 2012; Bonasio and
89 Shiekhattar, 2014; Chekanova, 2015; Ransohoff et al., 2018). This is true for either lincRNAs or
90 *cis*-NATs and applies to both animal and plant models. Well-characterized mechanisms by which
91 lncRNAs affect gene transcription include recruitment of chromatin or transcription regulators and

92 displacement of transcriptional repressors. Examples of such mechanisms in animals includes
93 inhibition of transcription via histone methylation by *HOTAIR* (Gupta et al., 2010) or DNA
94 methylation by *pRNA* (Schmitz et al., 2010), stimulation of transcription by the recruitment of the
95 activator PYGO2 by the lincRNA *PCGEM1* (Schmitz et al., 2010), and the displacement of the
96 repressive glucocorticoid response element by the lincRNA *Gas5* (Kino et al., 2010). Similar
97 mechanisms for lincRNAs in plants have been described, such as histone modification at the
98 flowering locus *FLC* triggered by the *cis*-NAT *COOLAIR* (Liu et al., 2010) or the intronic lincRNA
99 *COLDAIR* (Heo and Sung, 2011), as well as the transcriptional activation of pathogen-responsive
100 gene *PRI* via the recruitment of a Mediator component by lincRNA *ELF18* (Seo et al., 2017).
101 LincRNA can also interact with splicing factors to regulate alternative splicing, as described for
102 lincRNA *MALATI* in animals (Tripathi et al., 2010) and *ASCO* in plants (Bardou et al., 2014).
103 Moreover, lincRNA can control mRNA stability via interaction with members of the *Staufen*
104 double-stranded RNA (dsRNA)-binding proteins in animals (Gong and Maquat, 2011) or inhibition
105 of microRNA action on mRNA degradation via target mimicry, as described for the Arabidopsis
106 *IPSI* lincRNA involved in the response of plants to inorganic phosphate (Pi) deficiency (Franco-
107 Zorilla et al., 2007). Another mechanism for the decrease in steady-state mRNA level associated
108 with *cis*-NAT expression is the generation of siRNA via processing of double-stranded RNA
109 generated by the overlapping *cis*-NAT with its cognate sense mRNA (Khorkova et al., 2014).
110 However, considering the large number of potential *cis*-NAT:sense mRNA pairs in animal and plant
111 genomes, relatively few examples of siRNA-mediated effects for *cis*-NATs have been described,
112 indicating that this mechanism may be less frequently employed than initially thought.

113

114 In contrasts to the effects of lincRNA on transcription and mRNA levels, examples of modulation of
115 mRNA translation by lincRNA are rather rare. Examples involving lincRNAs in human cell lines are
116 the inhibition of translation of targets *CTNNB1* and *JUNB* via recruitment of the translational
117 repressor Rck by the lincRNA-p21 (Yoon et al., 2012) and the inhibition of *c-Myc* translation by the
118 recruitment of the eukaryotic initiation factor eIF4E by lincRNA *GAS5* (Hu et al., 2014). Repression
119 of mRNA translation was also demonstrated for the *cis*-NAT of the *PU.1* gene, encoding a
120 transcription factor in mammals (Ebraldize et al., 2008). Recently, three examples for the
121 enhancement of translation by *cis*-NATs have been described. In rice (*Oryza sativa*), expression of
122 the *cis*-NAT of the Pi exporter gene *PHO1;2* was shown to enhance the association of the cognate
123 mRNA to polysomes, leading to the accumulation of PHO1;2 protein despite unchanged steady-
124 state level of the corresponding mRNA (Jabnourne et al., 2013). In mice, *Uchl1* mRNA translation is
125 enhanced by a *cis*-NAT that is exported to the cytoplasm upon inhibition of the Target of
126 Rapamycin (TOR) pathway (Carrieri et al., 2012). Finally, the human regulator of megakaryocyte

127 differentiation *RBM15* is also translationally enhanced by a *cis*-NAT (Tran et al., 2016). Little is
128 known about the mechanisms of action of the three translation enhancer *cis*-NATs reported so far.
129 All three pairs are oriented in a head-to-head manner (5'-5'). For *RBM15*, the region of the antisense
130 overlapping with the sense mRNA 5'UTR alone was found to be sufficient to enhance translation
131 (Tran et al., 2016). In contrast, for *Uchl1*, two elements in the *cis*-NAT were found to be essential,
132 namely the region overlapping with the 5' end of *Uchl1* mRNA and a non-overlapping inverted
133 Short Interspersed Nuclear Element (SINE) B2 element, a class of retrotransposable repeat element
134 (Carrieri et al., 2012). More recently, *cis*-NATs containing distinct SINE elements have been
135 identified in mammals as potential translation enhancers (Schein et al., 2016), whereas expression
136 of some ribosome-associated *cis*-NATs in plants were correlated with increased mRNA translation
137 (Bazin et al., 2017).

138

139 The low number of *cis*-NATs experimentally validated to influence translation of the cognate
140 mRNA might reflect the fact that most genome-wide studies of *cis*-NATs examined the correlation
141 between steady-state level of mRNAs and the expression of *cis*-NATs, an approach that is not
142 suitable for studying translation. In the present study, we took advantage of the polysome profiling
143 method combined with strand-specific RNA sequencing to identify, in *A. thaliana* plants, *cis*-NATs
144 whose expression level were associated with a change of cognate sense mRNA level, as well as
145 translation across a range of experimental conditions. The impact of *cis*-NAT expression on cognate
146 mRNA translation was further validated by expression of several *cis*-NATs in transgenic *A.*
147 *thaliana* and/or by transient expression in protoplasts.

148

149

150
151

152 RESULTS

153 Experimental setup to identify *cis*-NATs associated with changes in mRNA level and mRNA 154 translation

155 In order to identify *cis*-NATs impacting their cognate sense mRNA transcript level as well as
156 mRNA translation, an experimental procedure was set up allowing the quantification of steady-state
157 levels of coding and non-coding RNAs along with the determination of mRNA translation
158 efficiency genome-wide in *A. thaliana* seedlings grown under various conditions. Whole seedlings
159 grown in liquid cultures in the presence of a high (1 mM) or low (100 μ M) concentration of Pi were
160 analyzed, as well as roots and shoots from seedlings grown on agar-solidified medium
161 supplemented with different phytohormones, namely auxin (indole acetic acid, IAA), abscisic acid
162 (ABA), methyl-jasmonate (MeJA) or 1-aminocyclopropane-1-carboxylic acid (ACC), a precursor
163 of ethylene. For each sample, steady-state levels of *cis*-NATs and mRNAs were determined by
164 strand-specific sequencing of total polyA⁺ RNA, whereas translation efficiency was assessed for the
165 same sample by sequencing polysome-associated RNA purified by centrifugation through sucrose
166 density gradients. Sequencing of each total or polysomal RNA sample yielded between 30 and 60
167 million paired-end reads. Three independent biological replicates were analyzed for each treatment,
168 and a total of at least 120 million paired-end reads were obtained per condition.

169

170 The genes up- or down-regulated in response to the different treatments were identified by pairwise
171 comparisons between hormone treated or low Pi samples and their corresponding controls. In
172 response to low Pi, 2,991 protein-coding genes (according to the TAIR10 annotation) were
173 significantly up-regulated with a fold change > 2 and adjusted p-value (adj.pval) < 0.1, and 2,149
174 were significantly down-regulated (Figure 1A, Supplemental Table S1-S2). Fewer genes were
175 differentially expressed in response to the different hormone treatments (Supplemental Figure S1,
176 Supplemental Table S1-S2). For example, upon auxin treatment, 377 and 120 protein-coding genes
177 were up-regulated in roots and shoots, respectively (Supplemental Table S2). Untreated root and
178 shoot tissues were also compared and their transcriptomes were dramatically different, as expected
179 for two different organs, with 3,906 and 4,742 protein-coding genes significantly up- or down-
180 regulated, respectively, in roots relative to shoots (Supplemental Table S2).

181

182 Quality assessment of the transcriptomic data was first performed by Gene Ontology (GO) term
183 enrichment analyses for each set of up-regulated genes. This analysis confirmed the strong
184 induction of marker genes associated with the different treatments. The genes up-regulated in
185 response to low Pi were significantly enriched for the GO term “cellular response to Pi starvation”
186 (GO:0016036 adj.pval=5.3x10⁻¹¹) (Supplemental Figure S2A). Among these, *Induced by Phosphate*

Figure 1

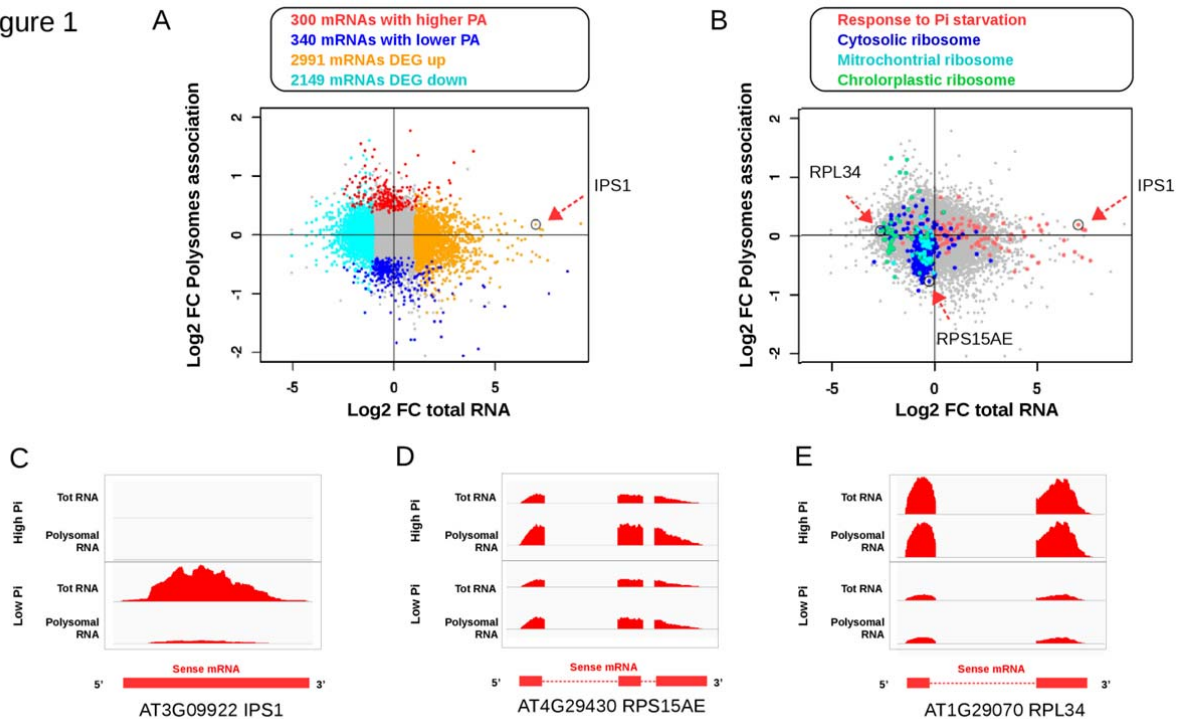


Figure 1. Steady state mRNA expression level and association with polysomes in response to grow of Arabidopsis to low Pi condition. **A:** Relation between log₂-fold change of mRNA steady-state level (x axis) is plotted against the log₂-fold change in polysome association (y axis). Coding genes significantly up- or down- regulated at the mRNA steady-state level are colored in yellow and cyan respectively, while mRNA significantly more or less associated with polysomes are colored in red and blue, respectively. The genes not showing any statistical difference are colored in grey. **B:** Same plot as A where genes associated with GO terms “Response to Pi starvation”, “Cytosolic ribosome”, “Mitochondrial ribosome”, and “Chloroplasmic ribosome” are colored in pink, dark blue, light blue and green, respectively. **C-E:** Normalized RNA-seq coverage plots for the *IPS1*, *RPS15AE* and *RPL34* genes. The two upper panels show the coverage plots for total mRNA and polysomal RNA from high Pi samples and the two lower panels correspond to low phosphate samples. The schematic exonic organization of each gene is represented by red boxes and lines below the plots.

187 *Starvation 1 (IPS1)*, a known highly induced marker of Pi deficiency, was strongly over-expressed
 188 (fold change=127.9, Figure 1A, C). Similarly, the up-regulated genes were significantly enriched in
 189 GO terms “response to abscisic acid” (GO:0009737, adj.pval=1.3x10⁻¹⁰), “response to auxin”
 190 (GO:0009733, adj.pval=6.5x10⁻¹¹), “jasmonic acid metabolic process” (GO:0009694,
 191 adj.pval=5.6x10⁻¹¹) and “ethylene-activated signaling pathway” (GO:0009873, adj.pval=6.4x10⁻⁸)
 192 in root samples treated with auxin, ABA, methyl jasmonate and ACC, respectively, compared to
 193 untreated roots (Supplemental Figure S2B-E).

194

195 The genes differentially expressed in response to low Pi and ABA treatments were further
 196 compared to previously published datasets (Supplemental Figure S3). Approximately 71% of the
 197 genes up-regulated in whole seedlings upon ABA treatment in the study of Song et al. (2016) were
 198 also up-regulated in ABA-treated roots and/or shoots in our dataset (941 genes out of 1,327).
 199 Similarly, 79% of genes up-regulated in the study of Bazin et al. (2017) (154 / 194) and 30.5% of
 200 genes up-regulated either in roots or shoot in Yuan et al. (2016) were common with the genes up-
 201 regulated under our low-Pi condition. The lower proportion of common differentially expressed
 202 genes with that reported by Yuan et al. (2016) might be explained by the differences in terms of

203 tissue analyzed (root versus whole seedlings) and growth conditions (e.g. liquid versus solid
204 medium and different Pi concentrations).

205

206 **Analysis of differential mRNA translation**

207 Translation efficiency of coding genes can be estimated by measuring the proportion of mRNA
208 molecules associated with polysomes relative to the amount of total RNA, as previously described
209 (Mustroph et al., 2009; Juntawong et al., 2014). Using sequencing data from polysome-associated
210 RNA, the ratio of polysome association (PA) was calculated for each gene by dividing the
211 normalized readcount in the polysomal RNA fraction by the normalized readcount measured for
212 total RNA steady-state level. The treated samples were compared to that in the corresponding
213 control conditions and loci with a 30% increase or decrease in PA ratio and an $\text{adj.pval} < 0.1$ were
214 considered differentially associated with polysomes, and thus potentially regulated translationally
215 (Supplemental Table S1, S3). In response to growth under low-Pi conditions, 300 and 340 protein-
216 coding genes were significantly more and less associated with polysomes, respectively, compared to
217 that under high-Pi conditions (Figure 1A). GO enrichment analyses revealed that the coding genes
218 with a lower association with polysomes in response to low Pi were strongly enriched for ribosomal
219 proteins (GO:0022626cellular component “cytosolic ribosome”, $\text{adj.pval}=2.26 \times 10^{-11}$) (Figure 1B,
220 Supplemental Figure S4A), such as the cytosolic ribosomal protein RPS15AE (Figure 1D). This
221 finding was consistent with that of previous reports, where a similar down-regulation of the
222 translation of the ribosomal proteins was observed by ribosome footprints in response to both Pi
223 deficiency (Bazin et al., 2017) and hypoxia (Juntawong et al., 2014), validating both techniques for
224 the analysis of mRNA translation. Of note, most of the genes constituting chloroplastic ribosomal
225 proteins, such as RPL34 (Figure 1B, E) showed a strong decrease in mRNA steady-state level
226 without significant change in PA. The genes encoding mitochondrial ribosomal proteins on the
227 other hand were globally less associated with polysomes, similarly to those encoding cytosolic
228 ribosomal proteins (Figure 1B).

229

230 Many genes were also found differentially associated with polysomes when comparing root and
231 shoot tissues (Supplemental Figure S5, Supplemental Table S3). For example, 946 protein-coding
232 genes were significantly more associated with polysomes in roots and 1,033 in shoots, in untreated
233 samples. Interestingly, the strongest enrichment within the set of genes with higher PA in shoots
234 corresponds to GO:0008380 “mRNA splicing” ($\text{adj.pval}= 6 \times 10^{-11}$) (Supplemental Figure S4B).
235 *SERRATE* and *SR45*, for example, were strongly associated with polysomes in shoots and very
236 poorly in roots (fold change PA = 5.3 and 4.2 for *SERRATE* and *SR45*, respectively), despite similar
237 steady-state levels of mRNA in both tissues (Supplemental Figure S5B-D). Both *SERRATE* and

238 SR45 have been experimentally validated to participate in splicing, with an additional role for
239 SERRATE in microRNA processing (Laubinger et al., 2008; Zhang et al., 2017).

240

241 ***De novo* identification of *cis*-NATs**

242 *Cis*-NATs expressed in response to the different treatments were identified using the pipeline
243 described in the Materials and Methods (Figure 2A). In this pipeline, pairs of protein-coding genes
244 having mRNAs that may overlap in a sense-antisense fashion are not included as *bona fide cis*-
245 NATs. *De novo* transcriptome annotations corresponding to each of the 12 experimental conditions
246 analyzed were merged, and, after comparison to the TAIR10.31 annotation (Berardini et al., 2015),
247 a novel set of 4,411 *cis*-NATs were identified. Approximately 9% (374) of these *cis*-NATs were
248 recently annotated in the Araport11 database (Cheng et al., 2017). We then used the FEELnc tool
249 (Wucher et al., 2017) (see Materials and Methods and Supplemental Materials and Methods for
250 details) to determine *in silico* the coding potential of all the newly identified *cis*-NATs. The large
251 majority of these *cis*-NATs (98.5%) were lacking coding potential and only 63 were predicted to be
252 potentially coding. This prediction of coding potential was well supported by our experimental
253 polysome profiling data since the *cis*-NATs predicted to be coding were significantly more
254 associated with polysomes than seen for the non-coding *cis*-NATs (Figure 2B). A similar difference
255 was observed when comparing protein-coding and non-coding genes annotated in the TAIR10
256 database.

257

258 Exploring the conservation across plant genomes of the peptides encoded by the 63 *cis*-NATs with
259 high coding potential, we identified a group of 10 peptides that were well conserved amongst plant
260 genomes, and a second group of nine peptides conserved amongst Brassicaceae species only
261 (Supplemental Figure S6). The remaining 44 predicted coding *cis*-NATs were poorly or not
262 conserved. Seven of the *cis*-NATs encoding conserved peptides (Group I or II) were recently
263 annotated as (putative) protein-coding genes in the ARAPORT11 database but not in TAIR10. The
264 transcripts encoding these evolutionary conserved peptides should thus likely be considered as
265 ~~new~~ novel protein-coding genes.

266

267 Expression of the identified *cis*-NATs was well supported by published epigenetic profiling data
268 from Jégu T. et al. (2017). The predicted transcription start sites of the *cis*-NATs were strongly
269 enriched for the activating histone mark H3K9Ac as well as micrococcal S7 nuclease (Mnase)
270 footprints to the same extent as that in TAIR10 protein-coding loci, confirming the transcriptionally
271 active state of the promoter regions of the *cis*-NATs (Supplemental Figure S7). Moreover, 60% of

Figure 2

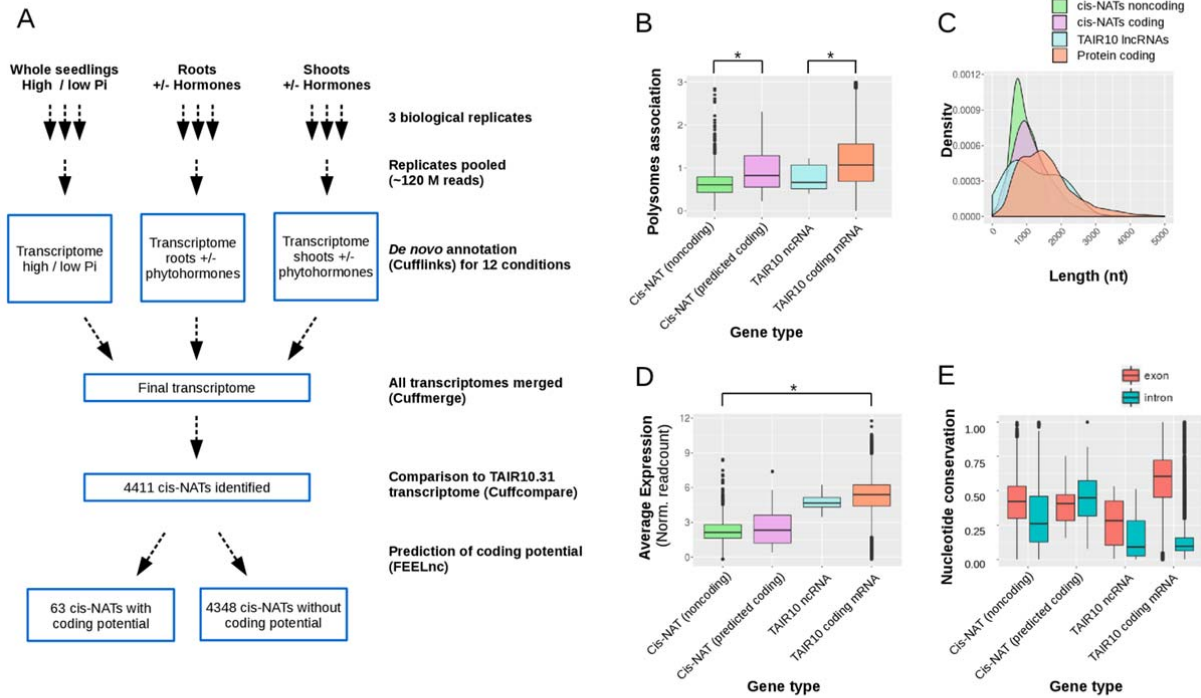


Figure 2: Identification and characterization of *cis*-NATs. **A:** Schematic diagram of the pipeline used for *de novo cis*-NAT identification from the 12 different experimental conditions. **B:** Boxplot comparing polysome association between *cis*-NATs predicted noncoding (green), or with coding potential (pink), ncRNA (cyan) and protein coding genes (salmon) annotated in TAIR10 database. **C, D:** Plots comparing transcript length (C) and RNA steady-state-level (D) between *cis*-NATs predicted noncoding (green), or with coding potential (pink), ncRNA (cyan) and protein coding genes (salmon) annotated in TAIR10 database. **E:** Boxplots comparing the nucleotide conservation across 20 angiosperm genomes within exonic and intronic regions of the four categories of transcripts listed above.

272 the *cis*-NATs detected in our dataset overlapped with *cis*-NATs previously identified in at least one
 273 of the three datasets used for comparison: the PlncDB database (Jin et al., 2013; Wang et al., 2014)
 274 as well as the work of Yuan et al. (2016) and Bazin et al. (2017)• (Supplemental Figure S8).

275

276 *Cis*-NATs were on average shorter, expressed at a lower level and had a weaker genomic sequence
 277 conservation (PHASTcons score) compared to that of TAIR10 annotated non-coding RNA and
 278 protein-coding mRNAs (Figure 2C-E), consistent with previous reports of *cis*-NATs in plants and
 279 other eukaryotes (Wang et al., 2005; Khorkova et al., 2014; Yuan et al., 2015). Furthermore, the
 280 polysome association value of *cis*-NATs was significantly lower (0.64) compared to that of mRNAs
 281 (1.19), but similar to that of the non-coding transcripts annotated in the TAIR10 database (0.54)
 282 (Figure 2B).

283

284 To validate our pipeline of identification of differentially expressed *cis*-NATs and protein-coding
 285 genes, we analyzed by RT-qPCR the expression level of six protein-coding genes and six *cis*-NATs
 286 predicted to be up- or down-regulated in response to phosphate starvation. For the 12 genes
 287 analyzed, the RT-qPCR results showed a significant increase or decrease in RNA steady-state level
 288 in agreement with the RNAseq data (Supplemental Figure S9).

289

290 ***Cis*-NATs associated with changes in steady-state level of their cognate mRNA**

291 To identify *cis*-NATs potentially regulating the expression of their cognate mRNA at the
292 transcriptional or translational level, we looked for correlation between expression levels of all
293 available *cis*-NATs (e.g. *cis*-NATs identified in this study and those included in TAIR10.31, total of
294 4,846 *cis*-NATs) and cognate sense mRNA steady-state levels or polysome association across the
295 different experimental conditions analyzed, comparing hormone treated samples with untreated
296 controls for root and shoot tissues as well as seedlings grown under low- or high-Pi conditions.
297 Untreated root and shoot tissues were also compared to identify *cis*-NATs potentially regulating
298 tissue-specific gene expression. All *cis*-NAT:sense mRNA pairs were put into four categories
299 considering their region of overlap, namely overlap in the 5' end, 3' end, completely included within
300 the sense region, or *cis*-NATs that extend beyond the 5' and 3' region of the coding sense
301 (overhanging) (Supplemental Figure S10).

302

303 Analysis for potential effects of *cis*-NAT expression on steady-state sense mRNA level was
304 performed. For each pairwise comparison, the *cis*-NAT:mRNA pairs were considered correlated if
305 both the *cis*-NAT and the cognate mRNA were differentially expressed, with a fold change of at
306 least 2 and a FDR < 0.1. A total of 1,310 *cis*-NATs, including 67 annotated in TAIR10, were
307 differentially expressed in at least one condition (Supplemental Table S1). For 107 of these loci,
308 steady-state level of the cognate mRNA was positively correlated to *cis*-NAT expression (Table 1,
309 Supplemental Table S4). For example, both the mRNA and the *cis*-NAT of the locus AT2G37580
310 were significantly up-regulated upon ABA treatment in shoots (FC= 2.13, adj.pval=0.029 for the
311 mRNA and FC=2.06, adj.pval=1.3x10⁻² for the *cis*-NAT) (Figure 3A). We also found 41 pairs with
312 a negative correlation, such as AT1G68940, whose mRNA was up-regulated in response to low-Pi
313 conditions (FC=2.16, adj.pval=7.9x10⁻³), whereas the *cis*-NAT was down-regulated (FC= 0.39,
314 adj.pval=7.2x10⁻²) (Figure 3B). Pearson correlation coefficient between *cis*-NAT and mRNA
315 expression was calculated across the 12 experimental conditions analyzed, taking advantage of the
316 whole experimental dataset to identify *cis*-NATs with stronger positive and negative expression
317 correlation with their cognate sense mRNA. This analysis revealed that 86 *cis*-NAT:sense mRNA
318 pairs out of 107 had a positive correlation coefficient higher than 0.4, whereas 27 *cis*-NAT:sense
319 mRNA pairs out of 41 had a negative correlation coefficient lower than -0.4, across all 12
320 experimental conditions (Figure 3E-F, Table 1).

321

322 **Identification of putative translation regulator *cis*-NATs**

Figure 3

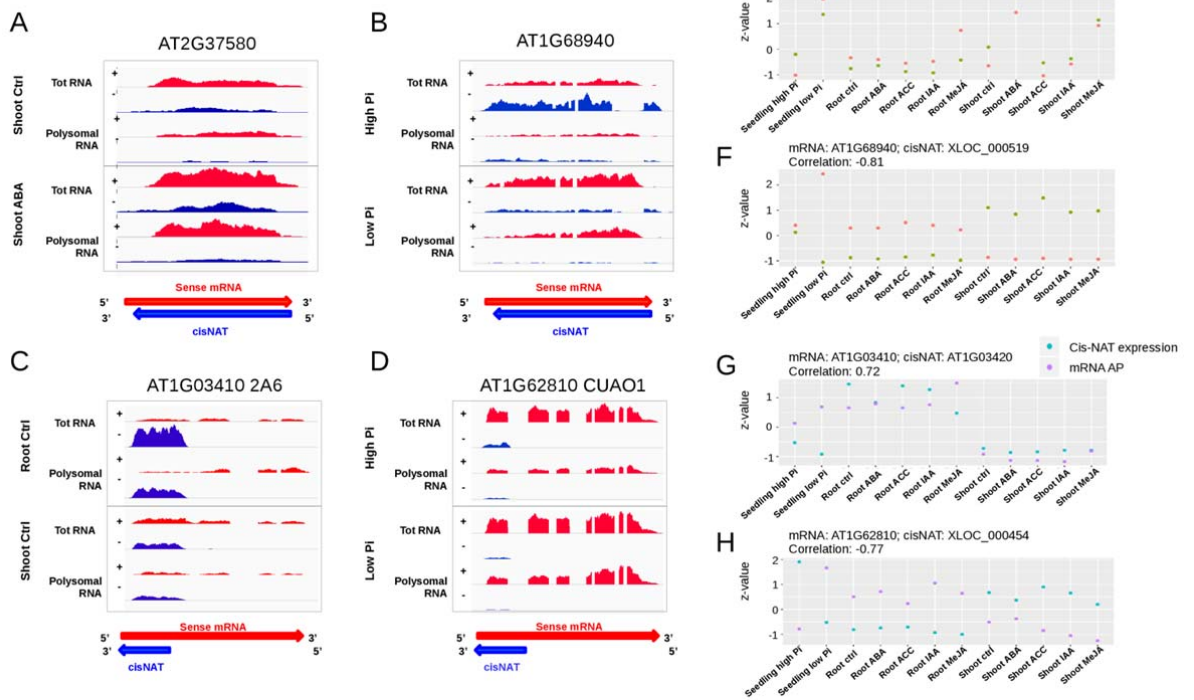


Figure 3: Correlations between expression of *cis*-NATs and changes in steady-state level or polysome association of the cognate sense mRNA. **A-D:** Coverage plots showing the density of RNA-seq reads per position at AT2G37580, AT1G68940, AT1G03410 and *CuAO1* loci. The red and blue areas represent the density of reads mapping to the sense mRNA and *cis*-NATs, respectively. For each experimental condition, the upper part corresponds to total RNA-seq reads and the lower part to polysomal RNA-seq reads. The red and blue arrows below indicate the *cis*-NAT-mRNA pair orientation. **E-H:** Correlation plots showing the steady-state level of the coding mRNA (red dots) and *cis*-NAT (green dots) for AT2G37580 and AT1G68940 loci (E and F, respectively) or the steady-state level of the *cis*-NAT (cyan dots) and the association with polysomes of the cognate sense mRNA (purple dots) for AT1G03410 and *CuAO1* loci (G and H, respectively). The Z-score of normalized read counts calculated from the 12 experimental conditions is represented on the Y-axis. Pearson correlation coefficients between the 2 variables shown in each plot are indicated on top of the plots.

323 In order to identify *cis*-NATs influencing the translation of their cognate sense
 324 for *cis*-NAT:sense mRNA pairs where the *cis*-NAT was differentially expressed (fold change > 2
 325 and $\text{adj.pval} < 0.1$) and the sense mRNA that was differentially associated with polysomes (at least
 326 30% increase or decrease, $\text{adj.pval} < 0.1$) in response to treatment. A finer filtering step was also
 327 performed using additional criteria such as the size of the overlapping region or the relative level of
 328 expression between *cis*-NAT and mRNA (see Material and Methods for further details). A total of
 329 eight *cis*-NAT:sense mRNA pairs were identified for which *cis*-NAT differential expression was
 330 positively correlated to mRNA differential association with polysomes in at least one pairwise
 331 comparison (Supplemental Table S4). For example, AT1G03410 mRNA was more associated with
 332 polysomes ($\text{FC}=1.79$, $\text{adj.pval}=0.01$) when the *cis*-NAT was more expressed ($\text{FC}=2.71$,
 333 $\text{adj.pval}=5.6 \times 10^{-18}$) in untreated roots samples compared to untreated shoots (Figure 3C). A total of
 334 six pairs showed a negative correlation between *cis*-NAT expression and cognate mRNA
 335 association with polysomes (Supplemental Table S4), including the *CuAO1* locus whose sense
 336 mRNA was more associated with polysomes ($\text{FC}=1.68$, $\text{adj.pval}=0.05$) when the *cis*-NAT was less
 337 abundant ($\text{FC}=0.29$, $\text{adj.pval}=1.3 \times 10^{-5}$) in Pi-deficient seedlings (Figure 3D). The expression of
 338 three out of the eight *cis*-NAT:sense mRNA pairs with a positive correlation and three out of the six
 339 pairs with negative correlation had a Pearson correlation coefficient > 0.4 and < -0.4, respectively,

340 with polysome association of their cognate mRNAs across the 12 experimental conditions (Figure
341 3G-H, Table 1, Supplemental Table S4).

342

343 The *cis*-NATs identified that positively or negatively correlated with sense mRNA steady-state
344 transcript level or polysome association were further analyzed for relation with miRNAs, i.e.
345 presence of miRNA precursor sequence, miRNA target sequence, and potential as a microRNA
346 target mimic (see Material and Methods). Out of the 4,846 *cis*-NATs analyzed, 14% (682) were
347 predicted to contain at least one miRNA binding site (Supplemental Table 1), including 7 and 14
348 *cis*-NATs negatively and positively correlated to cognate mRNA steady-state level, respectively
349 (Supplemental Table 1). Two *cis*-NATs positively correlated with mRNA polysome association
350 were predicted to contain miRNA binding sites, but none of the *cis*-NATs with a negative
351 correlation. Only seven *cis*-NATs were predicted as miRNA precursors and 69 contained potential
352 miRNA target mimic sites, including two *cis*-NATs positively correlated with cognate mRNA
353 expression and one *cis*-NAT positively correlated with mRNA polysome association (Supplemental
354 Table S1). No *cis*-NAT negatively correlated to mRNA expression or polysome association
355 contained a putative miRNA target mimic site.

356

357 We also took advantage of 40 publicly available small RNA datasets to analyze the *cis*-NATs in
358 relation to siRNAs. We identified 24,119,910 small reads between 18 and 28 nucleotides long
359 mapping to TAIR10 reference genome. Of those, 666,181 mapped to *cis*-NAT loci and were
360 considered as *cis*-NAT-siRNAs. Most of them were 21 and 24 nucleotides long (Supplemental
361 Figure S11A) and the overlapping region of *cis*-NATs showed a significantly higher density in
362 small RNAs compared to that of non-overlapping regions (Supplemental Figure S11B), in
363 agreement with previous reports (Zhou et al., 2009; Yuan et al., 2015). We identified 1336 potential
364 siRNA precursor *cis*-NATs, with at least five small reads mapping to the overlapping region and a
365 read density at least two-fold higher in the overlapping region than that in the non-overlapping
366 region. From this set of 1,336 *cis*-NATs, 25 belonged to the group of putative transcription
367 enhancers (representing 23% of the 107 candidates), 10 to the group of putative transcription
368 inhibitors (representing 24% of the 41 candidates), one to the group of putative translation
369 enhancers (representing 12.5% of the 8 candidate) and none to the group of putative translation
370 repressors (Supplemental Table S1).

371 We also looked for the presence of transposable elements or inverted repeats within the *cis*-NATs
372 identified (see Material and Methods) (Supplemental Table S1). Approximately 10.5% of the *cis*-

373 NATs (i.e. 508) contained at least part of transposable element sequences, including one positively
374 correlated and one negatively correlated to mRNA translation. Transposable element sequences
375 were found in 15 out of the 107 *cis*-NATs correlated with cognate mRNA steady-state level.
376 Similarly, we found that 121 *cis*-NATs contained inverted repeats, including one in a *cis*-NAT
377 positively correlated with cognate mRNA translation and one in a *cis*-NATs negatively correlated
378 with cognate mRNA steady-state level.

379

380 **Experimental validation of *cis*-NAT regulation of cognate sense mRNA translation**

381 A positive or negative correlation between *cis*-NAT expression and cognate mRNA association
382 with polysomes could indicate translation enhancement or repression of the mRNA by the *cis*-NAT.
383 To experimentally validate such a potential translation regulation activity, two *cis*-NATs with
384 potential translation enhancer activity and two with putative translation repressor activity were
385 cloned after the CaMV35S promoter and used to transform *A. thaliana* to produce transgenic lines
386 over-expressing the *cis*-NATs in *trans*. Two independent transgenic lines were selected for each *cis*-
387 NAT construct with a robust (>10-fold) over-expression of the transgenic *cis*-NAT compared to the
388 steady-state level of the endogenous *cis*-NAT in wild-type lines but without a significant change of
389 steady-state level of the endogenous cognate mRNA (Supplemental Figure S12). Polysome
390 association of each cognate sense mRNA was analyzed by sucrose density gradient in the lines
391 over-expressing the *cis*-NATs compared to that in a control line transformed with an empty vector.
392 The distribution of mRNAs along the sucrose density gradient was determined by RT-qPCR (Figure
393 4B and E, 5B and E, and Supplemental Figure S13). In order to quantify the changes in terms of
394 association with polysomes in a more robust manner, the proportion of mRNA present either in
395 fractions containing free mRNA or monosomes (fractions 1 to 3) versus fractions containing
396 polysomal mRNAs (fractions 4 to 6) was calculated for each of the eight independent biological
397 replicates (Figure 4C and F, 5C and F). This analysis revealed that over-expression of the *cis*-NAT
398 associated with the *CuAOI* locus was associated with a decrease in translation of the cognate
399 mRNA (Figure 4B, C), in agreement with the negative correlation between *cis*-NAT steady-state
400 level and mRNA polysome association (Figure 4A). In contrast, polysome association of the mRNA
401 of locus At1g54260, encoding a potential transcription factor, was not significantly changed by the
402 over-expression of its *cis*-NAT in *trans* (Figure 4E, F), despite the positive correlation (Figure 4D).

403

404 Similar analysis performed for two *cis*-NATs that displayed positive correlation with their cognate
405 mRNA translation (Figure 5A, D) showed that lines over-expressing the *cis*-NAT to locus
406 At3g26240 showed a reproducible shift of the its cognate mRNA towards the heavy polysome

Figure 4

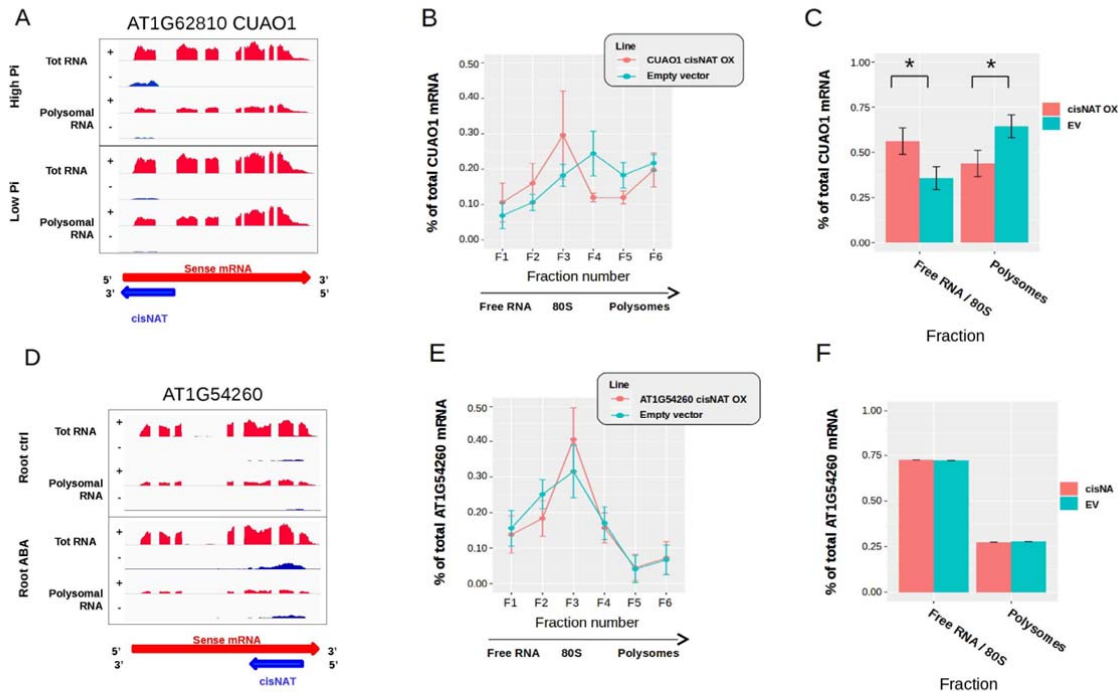


Figure 4: Expression of putative translation repressor *cis*-NATs in transgenic *A. thaliana*. **A and D:** Coverage plots showing the density of RNA-seq reads per position for the *CuAO1* (A) and AT1G54260 (D) loci, with the red and blue areas representing the sense mRNA and *cis*-NATs, respectively. **B and E:** Polysome profiles showing the proportion of endogenous mRNA in each of the 6 fractions of the sucrose gradient for transgenic lines over-expressing the *cis*-NAT (red) versus control lines transformed with an empty vector (turquoise) for the *CuAO1* (B) and AT1G54260 (E) sense mRNA-*cis*-NAT pair. **C and F:** Proportion of mRNA present in the first three fractions (free RNA and monosomes) and in the last three fractions (polysomes) of the gradient, in transgenic lines over-expressing *cis*-NAT (red) and in control lines transformed with an empty vector (turquoise) for the *CuAO1* (C) and AT1G54260 (F) sense mRNA-*cis*-NAT pair. Data in B, C, E and F represent the average between 8 independent biological replicates obtained with 2 independent transgenic lines. The error bars represents the confidence intervals with $\alpha=0.05$. The significant differences (Student test with p value <0.05) are indicated by a star.

407 fractions in eight independent biological replicates, indicating a stimulatory effect of *cis*-NAT
 408 expression on translation (Figure 5B, C). In contrast, over-expression of the *cis*-NAT to locus
 409 *WRKY45* (AT3G01970) did not change significantly the polysome profile of its cognate sense
 410 mRNAs (Figure 5E, F).

411

412 A protoplast co-transformation system was developed to independently validate the effects of *cis*-
 413 NAT expression on the translation of their cognate sense mRNA. Protoplasts were transformed with
 414 a plasmid containing a sense-coding gene fused to NanoLuc luciferase (Nluc), in the presence or
 415 absence of a plasmid expressing the cognate *cis*-NAT. The sense-Nluc vectors contained also an
 416 independent expression cassette for the firefly luciferase (Fluc), used as an internal transformation
 417 and loading control (see Materials and Methods for further details). The ratio Nluc:Fluc activity was
 418 used to assess the effect of each selected *cis*-NAT on its sense-encoded protein accumulation.
 419 Increasing the molar amounts of *cis*-NAT_{CuAO1} resulted in a corresponding decrease in the
 420 expression of the CuAO1-Nluc fusion protein as detected by a decrease in the Nluc:Fluc ratio
 421 (Figure 6A). Importantly, this inhibitory effect was not observed at the transcript level
 422 (Supplemental Figure S14). Similarly, increasing amounts of *cis*-NAT_{AT1G54260} resulted in reduction

Figure 5

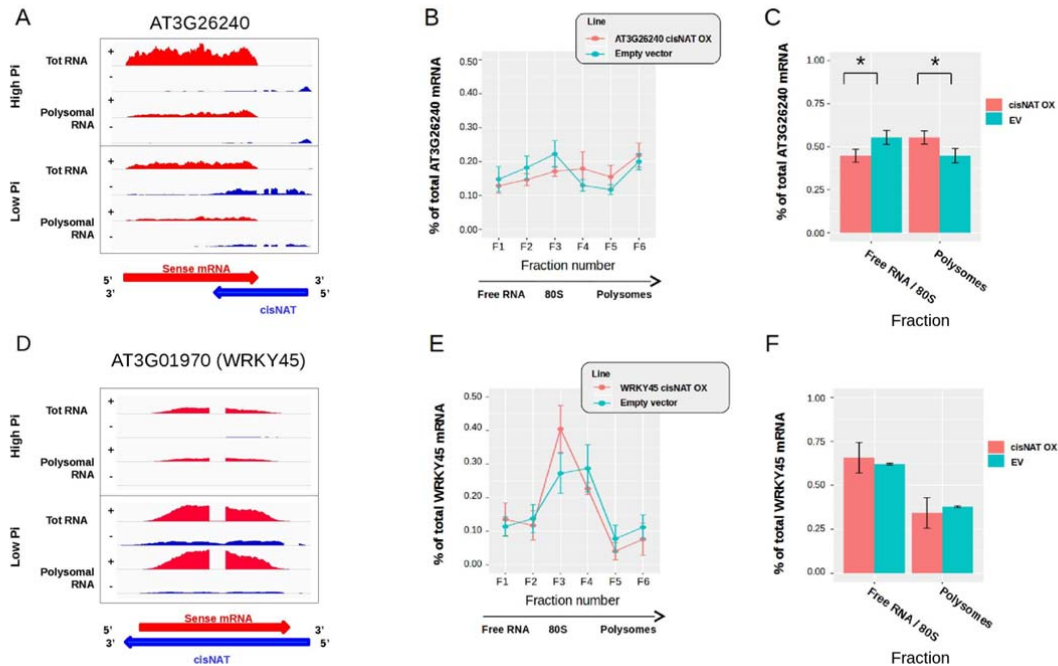


Figure 5: Expression of putative translation activator *cis*-NATs in transgenic *A. thaliana*. **A and D:** Coverage plots showing the density of RNA-seq reads per position for the AT3G26240 (A) and *WRKY45* (D) loci, with the red and blue areas representing the sense mRNA and *cis*-NATs, respectively. **B and E:** Polysome profiles showing the proportion of endogenous mRNA in each of the 6 fractions of the sucrose gradient for transgenic lines over-expressing the *cis*-NAT (red) versus control lines transformed with an empty vector (turquoise) for the AT3G26240 (B) and *WRKY45* (E) sense mRNA-*cis*-NAT pair. **C and F:** Proportion of mRNA present in the first three fractions (free RNA and monosomes) and in the last three fractions (polysomes) of the gradient, in transgenic lines over-expressing *cis*-NAT (red) and in control lines transformed with an empty vector (turquoise) for the AT3G26240 (C) and *WRKY45* (F) sense mRNA-*cis*-NAT pair. Data in B, C, E and F represent the average between 8 independent biological replicates obtained with 2 independent transgenic lines. The error bars represents the confidence intervals with alpha=0.05. The significant differences (Student test with pvalue <0.05) are indicated by a star.

423 in expression of the AT1G54260-Nluc fusion protein (Figure 6B) without an effect on transcript
 424 level (Supplemental Figure S14), although the effect was less pronounced than the one observed for
 425 the *cis*-NAT_{CuAOI}-sense construct pair. These later results are in contrast to the lack of significant
 426 effect observed in stable transgenic lines overexpressing *cis*-NAT_{AT1G54260} and analyzed by
 427 quantification of polysomal mRNA in sucrose gradient fractions (Figure 4E and F). Such
 428 discrepancy may reflect the higher variability of the transgenic-polysomal approach or the higher
 429 sensitivity of the protoplast transformation method. To further validate the specificity of the effects
 430 of *cis*-NAT on translation of the corresponding sense mRNA, *cis*-NAT_{CuAOI} was co-transformed
 431 with the AT1G54260-Nluc construct, and *cis*-NAT_{AT1G54260} was co-transformed with the *CuAOI*-
 432 Nluc construct. In this *cis*-NAT swap experiment, no effect on Nluc:Fluc ratio were observed
 433 (Figure 6C and 6D), revealing that the inhibitory effect of *cis*-NAT_{AT1G54260} and *cis*-NAT_{CuAOI} on
 434 translation was specific to their cognate sense genes.

435

436 The protoplast system was also used to test the two *cis*-NATs acting as potential translational
 437 enhancers that were previously analyzed in transgenic plants, namely the *cis*-NATs to AT3G26240
 438 and *WRKY45*, as well as an additional third candidate, *2A6* (AT1G03410) (Figure 7). There was a
 439 significant increase in Nluc:Fluc ratio upon addition of increasing amount of *cis*-NAT_{AT3G26240} to its

Figure 6

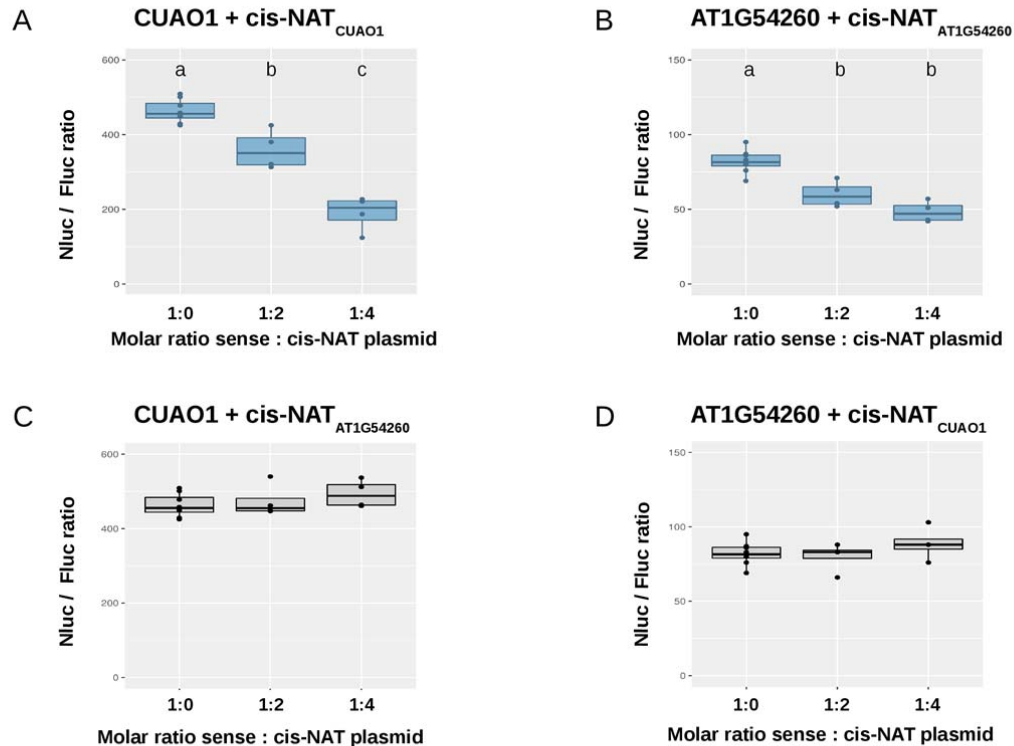


Figure 6. Transient expression of putative translation repressor *cis*-NATs in protoplasts. Arabidopsis leaf protoplasts were co-transformed with a plasmid combining a sense mRNA-NanoLuc luciferase (Nluc) fusion and a firefly luciferase (Fluc) along with various molar ratios of an independent plasmid for expression of a *cis*-NAT. The ratio of Nluc over Fluc activity is plotted for each combination of sense and *cis*-NAT plasmids. (A) Co-expression of *CuAO1*-Nluc fusion with its cognate *cis*-NAT. (B) Co-expression of AT1G54260-Nluc with its cognate *cis*-NAT. (C) Co-expression of *CuAO1*-Nluc with the *cis*-NAT to AT1G54260. (D) Co-expression of AT1G54260-Nluc with the *cis*-NAT to *CuAO1*. Statistical significant differences (t-test, p-value < 0.05; four biological replicates) between treatments are indicated distinct letters above the bars.

440 cognate sense construct, without a corresponding increase in transcript levels (Figure 7A and
 441 Supplemental Figure S14), confirming the translational enhancement of this *cis*-NAT. Similar to the
 442 results obtained with stable transgenic plants (Figure 5E, F), there was no significant effect of
 443 addition of *cis*-NAT_{WRKY45} on the expression of the *WRKY45*-Nluc construct (Figure 7C). Although
 444 we did not generate transgenic lines to test the effect of *cis*-NAT_{2A6} on the translation of its cognate
 445 sense mRNA, protoplast analysis revealed an increasing Nluc:Fluc ratio associated with the
 446 addition of *cis*NAT_{2A6} to its corresponding sense 2A6-Nluc construct, without changes in mRNA
 447 levels (Figure 7B and Supplemental Figure S14), revealing a similar translational enhancement
 448 effect as those observed with *cis*-NAT_{AT3G26240}. A swap experiment performed between the *cis*-
 449 NAT_{AT3G26240} and *cis*-NAT_{2A6} showed no enhancement effect on unrelated sense-Nluc fusion
 450 (Figure 7D-E), confirming that the stimulatory effect of *cis*-NAT_{AT3G26240} and *cis*-NAT_{2A6} on
 451 translation was specific to their cognate sense genes.

452

453 Over-expression of the putative translation inhibitor *cis*-NAT_{CuAO1} in transgenic lines probably
 454 resulted in lower levels of endogenous *CuAO1* protein although we were not able to detect and
 455 quantify reliably *CuAO1* protein by targeted mass spectrometry using N¹⁵-labeled plants (Hart-

Figure 7

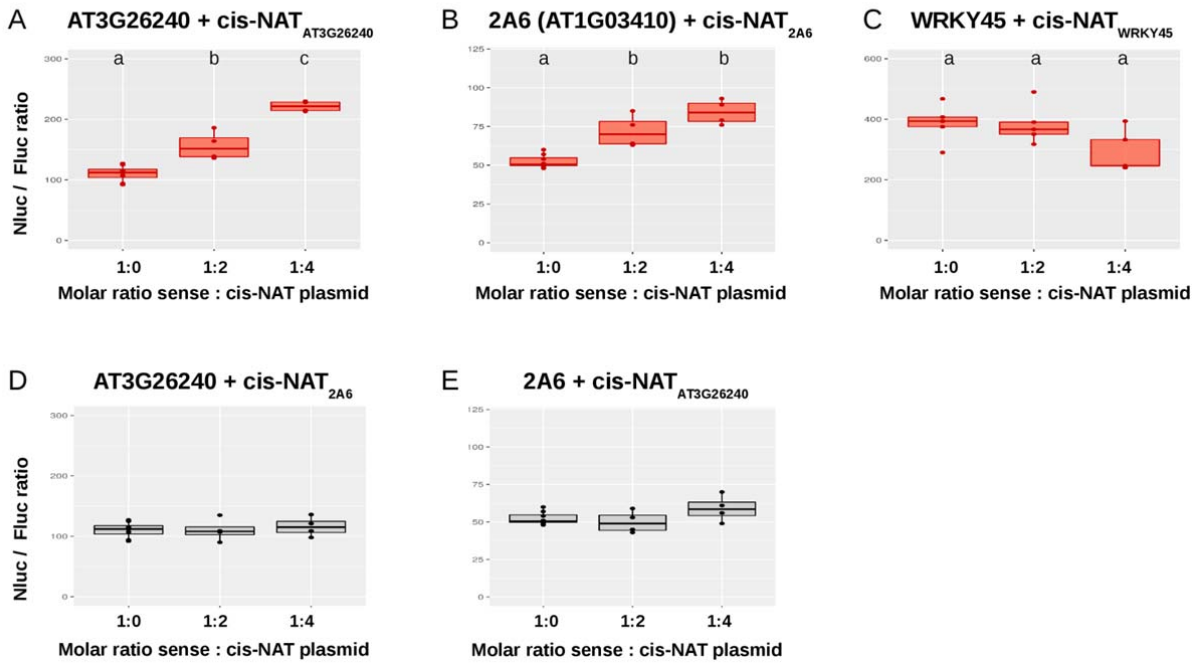


Figure 7. Transient expression of putative translation activator *cis*-NATs in protoplasts. Arabidopsis leaf protoplasts were co-transformed with a plasmid combining a sense mRNA-NanoLuc luciferase (Nluc) fusion and a firefly luciferase (Fluc) along with various molar ratios of an independent plasmid for expression of a *cis*-NAT. The ratio of Nluc over Fluc activity is plotted for each combination of sense and *cis*-NAT plasmids. (A) Co-expression of AT3G26240-Nluc fusion with its cognate *cis*-NAT. (B) Co-expression of 2A6 (AT1G03410)-Nluc with its cognate *cis*-NAT. (C) Co-expression of WRKY45 (AT3G01970)-Nluc with its cognate *cis*-NAT. (D) Co-expression of AT3G26240-Nluc with the *cis*-NAT to 2A6. (E) Co-expression of 2A6-Nluc with the *cis*-NAT to AT3G26240. Statistical significant differences (t-test, p-value < 0.05; four biological replicates) between treatments are indicated distinct letters above the bars.

456 Smith et al., 2017). Since Arabidopsis CuAO1 knock-down mutants were shown to be impaired
 457 in NO production induced by polyamines (Wimalasekera et al., 2011), we undertook to
 458 quantify NO production upon spermidine treatment in two independent *cis*-NAT_{CuAO1} over-
 459 expressing transgenic lines along with a CuAO1 T-DNA knock-down mutant. NO production
 460 was strongly impaired in CuAO1 knock-down mutant, in agreement with the previous results of
 461 Wimalasekera et al. (2011), but also in the *cis*-NAT_{CuAO1} over-expressing line #1
 462 (Supplemental Figure S15). The second *cis*-NAT over-expressing line also showed a
 463 reproducible reduction in NO production compared to that in the Col0 control although the
 464 associated p-value was above 0.05 (0.13).

465
 466
 467

469 **Discussion**

470

471 Out of a total set of 4,846 *cis*-NATs identified in this study or annotated in TAIR10, 157 (3.24%)
472 were found to have a potential to regulate the expression of their cognate sense mRNA based on
473 positive or negative correlations with either the steady-state mRNA level or polysome association.
474 The great majority of those potential regulatory *cis*-NATs (147 out of 157; Table 1) were associated
475 with changes in the transcript level of the cognate sense mRNA, with a stronger bias towards
476 concordant expression (107 out of 147). This bias towards concordance is somewhat surprising
477 since negative effect of *cis*-NAT expression on steady-state mRNA level is more commonly
478 described in the literature than positive effects (Khorkova et al., 2014). It is possible that
479 phenotypes associated with the disruption of *cis*-NATs with discordant expression pattern may be
480 more apparent than for concordant expression pattern. Furthermore, co-expression of *cis*-NAT and
481 cognate sense mRNA could, in many cases, be simply a consequence of local changes in chromatin
482 state encompassing a whole locus that would equally affect the access of the transcription
483 machinery to both the sense and antisense promoters, and thus would not be associated with a
484 regulatory mechanism for controlling sense mRNA expression. However, numerous examples exist
485 in the literature showing that increased expression of a *cis*-NAT may negatively affect sense mRNA
486 steady-state level via changes in histone marks localized primarily at the promoters of the sense
487 genes (Khorkova et al., 2014). Whereas fewer examples of similar local effect only on the promoter
488 activity of the sense genes have been described for *cis*-NATs having concordant expression pattern
489 (Mondal et al., 2010), more examples may be found through a more systematic analysis of this
490 group of *cis*-NATs in Arabidopsis.

491

492 Non-coding RNAs, and particularly lincRNAs, can regulate the expression of coding mRNA by
493 either masking a miRNA binding site via base pairing or by acting as a miRNA mimic (Wang et al.,
494 2013; Cho and Paszkowski, 2017). At least one example has been described in animals for a *cis*-
495 NAT masking a miRNA binding site present in the cognate sense gene (Faghihi et al., 2010). In the
496 present study, 600 sense genes associated with a *cis*-NAT were found to be a potential target for a
497 microRNA and 69 *cis*-NATs were found to contain a sequence that could act as a miRNA mimic
498 (Supplemental Table S1). Of those, only two *cis*-NATs were found in the group associated with
499 changes in steady-state mRNA level (both concordant) and only one associated with changes in
500 mRNA polysome association, namely *cis*-NAT_{WRKY45}. However, the effect of *cis*-NAT_{WRKY45} in its
501 cognate sense RNA could not be experimentally validated either in transgenic plants nor in
502 protoplasts (Figure 5D and 7C). Thus, whereas it is possible that some plant *cis*-NATs may function
503 in miRNA masking or as a miRNA mimic, it would not appear to be common.

504

505 Overlap between *cis*-NATs and their cognate sense mRNAs can potentially generate siRNAs
506 leading to gene silencing. There are several examples of *cis*-NATs down-regulating the cognate
507 mRNA level via a siRNA-mediated silencing pathway, including in Arabidopsis (Held et al., 2008;
508 Ron et al., 2010). It is thus possible that some of the *cis*-NATs identified in this study are potential
509 transcription inhibitors and the associated *cis*-NAT-siRNAs may act through a siRNA pathway.
510 There is also an example in Arabidopsis where *cis*-NAT expression leads to an increase in cognate
511 sense mRNA transcript via the generation of *cis*-NAT-siRNAs that inhibit the action of a
512 microRNA targeting the same cognate sense mRNA, thus leading to an increase in sense mRNA
513 level (Gao et al., 2015). Such a mechanism could potentially apply to three genes having *cis*-NATs
514 identified as potential transcription enhancers and associated with *cis*-NAT-siRNAs, namely
515 At1g23090, At2g44430 and At2g45850, which could be targeted by miR826a, miR838 and
516 miR837, respectively. In contrast, the only gene with a *cis*-NAT generating *cis*-NAT-siRNAs that
517 belongs to the group of potential translation regulators does not harbor miRNA targets.

518

519 *In silico* analysis of the set of *cis*-NATs identified a small group of 63 *cis*-NATs that had a higher
520 coding potential and that were more associated with polysomes than were other non-coding RNAs.
521 Further analysis revealed that 19 of those *cis*-NATs could encode polypeptides that were conserved
522 either mainly in Brassicaceae (Group II, 9 *cis*-NATs) or more broadly in plants (Group I, 10 *cis*-
523 NATs) (Supplemental Figure S6). Only one out of these 63 *cis*-NATs was positively correlated with
524 change in sense mRNA steady-state level (*cis*-NAT_{AT1G69260}), but none were correlated with
525 changes in mRNA translation (Supplemental Table S1). Association of mRNA with polysomes
526 does not directly show if the RNA is being actively translated into a polypeptide. However, analysis
527 of RNA translation by ribosome footprint in both plants and animals have revealed that a
528 remarkably broad spectrum of RNAs previously thought to be non-coding are actively being
529 translated by ribosomes (Aspden et al., 2014; Ji et al., 2015; Hsu et al., 2016; Bazin et al., 2017).
530 Recent analysis of non-coding RNAs in Arabidopsis roots revealed that 568 out of 1,676 *cis*-NATs
531 had ribosome footprints consistent with translation (Bazin et al., 2017). Interestingly, translation of
532 a small ORF present in a tasiRNA was shown to enhance tasiRNA production (Bazin et al., 2017),
533 suggesting that whereas many lincRNAs and *cis*-NATs may indeed be translated into peptides, the
534 act of translation itself rather than the specific sequence of the polypeptide may, in some cases, be
535 the predominant mechanism of regulation. In that context, four *cis*-NATs found by Bazin et al.
536 (2017) to have ribosome footprints are included in the group of 19 *cis*-NATs with coding potential
537 that are well conserved in plants (Supplemental Figure S6). These four *cis*-NATs may be good
538 candidates for transcripts coding for biologically active polypeptides.

539

540 In contrast to numerous reports of the effects of *cis*-NAT expression on sense gene transcription
541 and/or transcript stability, very few examples of *cis*-NATs affecting the translation of their cognate
542 sense mRNA have been described. Repression of mRNA translation by a *cis*-NAT has only been
543 described for the *PU.1* gene in mouse (Ebralidze et al., 2008), whereas *cis*-NATs enhancing cognate
544 mRNA translation have been reported for the rice *PHO1.2*, the mouse *Uchl1* and the human *RBM15*
545 genes (Carrieri et al., 2012; Jabnourne et al., 2013; Tran et al., 2016). A major goal of this work has
546 thus been to systematically explore the role of *cis*-NAT expression on translation of their cognate
547 mRNA in Arabidopsis. A total of 14 candidate *cis*-NATs with putative repressive or stimulatory
548 effects on cognate mRNA translation were found, which is 10-fold less compared to the number of
549 *cis*-NATs with effects on mRNA steady-state level. Analysis of the configuration of the *cis*-NATs
550 relative to the sense mRNA showed that *cis*-NATs associated with either translational stimulation
551 or repression had a higher proportion of head-to-head configuration compared to that of all other
552 *cis*-NATs (Supplemental Figure S10), although the low number of *cis*-NATs associated with
553 translation makes this distinction not statistically significant. Furthermore, some of the Arabidopsis
554 *cis*-NATs that were experimentally confirmed to affect translation have other configurations, such
555 as tail-to-tail (AT1G54260, AT3G26240).

556

557 The effects of *cis*-NAT expression on cognate mRNA translation were experimentally tested by
558 either stable transformation in plants and/or transient expression in leaf protoplasts for 5 of the 14
559 candidates. Four of those were validated, namely two *cis*-NATs mediating translational repression
560 (*CuAO1* and AT1G54260) and two *cis*-NATs mediating translational stimulation (AT3G26240 and
561 AT1G03410). These results highlight the robustness of the experimental pipeline used to identify
562 the candidates.

563

564 *CuOAI* encodes a copper amine oxidase involved in the catabolism of polyamines (Wimalasekera
565 et al., 2011). *CuAO1* has been shown to be involved in the generation of nitric oxide, a key
566 signaling molecule involved in a wide range of functions in plants, including seed germination, root
567 development and ABA-induced stomatal closure (Besson-Bard et al., 2008). The Arabidopsis
568 *cuaol-1* T-DNA knock-down mutant shows reduced production of NO after treatment with
569 spermidine (Wimalasekera et al., 2011). Several stress conditions are known to induce NO
570 synthesis, including phosphate deficiency (Sun et al., 2016). Although proteomic experiments could
571 not reliably quantify the amount of CuAO1 protein in transgenic lines overexpressing *cis*-
572 NAT_{*CuAO1*}, the same lines did show reduced NO production to levels similar to that of the *cuaol-1*
573 mutant, supporting an inhibitory effect of *cis*-NAT_{*CuAO1*} expression on CuAO1 production
574 (Supplemental Figure S15).

575

576 AT1g54260 harbors a highly conserved central globular domain (GH1) present in the linker histone
577 H1, proteins that perform important functions on chromatin structure and influencing accessibility
578 of trans-acting factors to DNA (Hergeth and Schneider, 2015; Kotlinski et al., 2017). The GH1
579 domain is known to bind DNA and the AT1G54260 protein belongs to the winged helix family of
580 DNA binding proteins. Beside histones H1, proteins containing GH1 domain have been shown to
581 binds to DNA, including at the telomeres, and potentially act at various level in the regulation of
582 chromatin structure (Zhou et al., 2016). The *cis*-NAT to AT1G54260 is up-regulated by both ABA
583 and low Pi (Supplemental Table S1). Modulation of AT1G54260 protein synthesis via expression
584 of its *cis*-NAT could thus have broad impact on chromatin structure and gene regulation under
585 various stress.

586

587 AT3G26240 encodes a protein of unknown function. AT1g03410 (*2A6*) encodes a protein
588 containing a domain associated with oxoglutarate and iron-dependent dioxygenase. In plants,
589 enzymes containing this domain catalyze the formation of plant hormones, such as ethylene,
590 gibberellins, anthocyanidins and pigments such as flavones. The *cis*-NAT_{AT1G03410} is of particular
591 interest since it corresponds to a retroelement of the *Sadhu* family (Rangwala and Richards, 2010).
592 The stimulatory activity of the *cis*-NAT of the mouse *Uchl1* on translation was shown to be
593 dependent on the SINEB2 retroelement (Carrieri et al., 2012). *Sadhu* retroelements resemble SINEs
594 in their structure, except that they do not contain similarity to known non-coding RNAs, such as
595 5SrRNA or tRNAs (the SINEB2 element is derived from a tRNA) (Weiner, 2002). Whereas the *cis*-
596 NATs of both *Uchl1* and AT1g03410 are in the head-to-head configuration, the SINEB2 element of
597 *cis*-NAT_{*Uchl1*} is located at the non-overlapping 3' end of the *cis*-NAT and *cis*-NAT_{AT1G03410} is almost
598 completely overlapping with the 5'UTR region of the sense mRNA except for the last 56
599 nucleotides (Supplemental Figure S16) (Carrieri et al., 2012). Whether or not SINEB2 elements and
600 *Sadhu* retrotransposon stimulates mRNA translation by a similar mechanism remains to be
601 determined.

602

603 The success of the validation methods relying on stable expression of *cis*-NATs in transgenic plants
604 or transient expression in protoplast reveals that the effect of *cis*-NAT expression on sense mRNA
605 translation can occur in *trans*. This implies that the *cis*-NAT produced from a distinct locus must be
606 sufficiently stable to locate and anneal to its target mRNA and recruit or sequester factors that affect
607 translation. This may, however, not always be the case, since the effects of some *cis*-NATs on
608 mRNA transcript level have been found to occur only in *cis* and not in *trans* (Fedak et al., 2016;
609 Rosa et al., 2016). Thus experimental validation of some *cis*-NATs for regulation of sense mRNA

610 translation may, in some cases, require other methods working in *cis*, such as precise mutation of
611 the *cis*-NAT locus by CRISPR/Cas9.

612

613 In conclusion, the experimental pipeline described in this work identified and validated a number of
614 novel *cis*-NATs in *Arabidopsis* that influence cognate sense mRNA translation. Although the
615 proportion of *cis*-NATs associated with changes in mRNA translation was relatively low compared
616 to the total number of *cis*-NATs expressed in the genome, it is likely that more candidates will be
617 found when plants are grown under different experimental conditions that lead to greater spectrum
618 of *cis*-NAT expression. Considering that a broad range of mechanisms have been identified for the
619 effect of lincRNAs and *cis*-NATs on transcriptional regulation, it is likely that the mechanisms
620 through which *cis*-NATs enhance or repress translation will also be quite diverse.

621

622 **Materials and Methods**

623

624 **Plant materials**

625 *A. thaliana* seeds (Col0) were germinated in half-strength Murashige and Skoog (MS) liquid
626 medium containing 1 mM (high) or 100 μ M (low) Pi. On day 5 and 6 after germination, the medium
627 was replaced to maintain a constant level of Pi. On day 7, whole seedlings were harvested and used
628 for total RNA extraction and polysome profiling. *A. thaliana* seeds were also germinated on agar-
629 solidified half-strength MS medium for 10 days, after which the seedlings were flooded with a
630 solution of half-strength MS containing 5 μ M IAA, 10 μ M ABA, 10 μ M MeJA, 10 μ M ACC, or no
631 hormone for the untreated control. After 3 h of incubation, roots and shoots were split and harvested
632 separately. For each of the 12 experimental conditions, 3 independent biological replicates were
633 carried out at different times.

634

635 **Total and polysomal RNA extraction**

636 Plant samples (whole seedlings, roots or shoots) were flash frozen and ground in a mortar and
637 pestle, and the polysomes were extracted essentially as described in Mustroph et al. (2009) with
638 minor modifications (see Supplemental Materials and Methods).

639

640 **Library preparation and RNA sequencing**

641 From each total and polysomal RNA sample, strand specific libraries were prepared using the
642 TruSeq Stranded Total RNA kit (Illumina) and polyA⁺ RNAs were selected according to
643 manufacturer's instructions. The libraries were sequenced on a HiSeq 2500 Illumina sequencer and
644 about 30 million of paired-end reads per sample were obtained. In total, about 120 million reads
645 were obtained for each of the 12 experimental conditions.

646

647 **Identification of *cis*-NATs and analysis of their coding potential**

648 To identify *cis*-NATs, the paired-end reads from the 3 replicates were pooled together and uniquely
649 mapped to the TAIR10 genome using Hisat2 (Kim et al., 2015). For each of the 12 conditions, the
650 transcriptome was determined *de novo* with Cufflinks (Trapnell et al., 2010), using the TAIR10.31
651 annotation as guide. The 12 annotation files obtained were merged using the Cuffmerge tool
652 (Trapnell et al., 2010). This transcriptome was then compared to TAIR10.31 using Cuffcompare
653 (Trapnell et al., 2010), and transcripts antisense to TAIR10.31 coding genes (class_code_x) were
654 considered as putative *cis*-NATs. The readcount for each TAIR10.31 protein coding gene and each
655 identified *cis*-NATs was determined using HTSeq-count (mode Union) and the identified *cis*-NATs
656 with a ratio read count *cis*-NAT / coding gene < 0.01 were discarded as false positives likely due to
657 imperfect strand specificity of the library preparation protocol (99.9%).

658

659 The “FEELnc codpot” module from FEELnc (version 0.01) (Wucher et al., 2017) was used to
660 identify *cis*-NATs that could potentially be coding for polypeptides (see Supplemental Material and
661 Methods).

662

663 **Characterization of *cis*-NATs**

664 Basic features such as length or GC content of transcripts, average steady-state levels or polysome
665 association were determined for each *cis*-NAT using custom functions written in Python. To
666 analyze the nucleotide conservation, PHASTcons scores were extracted from the 20 angiosperm
667 genome alignment as described by Hupaló et al. (2013). For each transcript, the average
668 PHASTcons score was calculated for exonic and intronic sequences. The presence of inverted
669 repeats was determined using the einverted program (EMBOSS;
670 <http://emboss.bioinformatics.nl/cgi-bin/emboss/einverted>) using default parameters. The presence
671 of miRNA binding sites within *cis*-NATs and coding transcripts was determined using
672 psRNATarget server (<http://plantgrn.noble.org/psRNATarget/>) with an expectation ≤ 3 and
673 unpaired energy (UPE) ≤ 25 . Potential miRNA precursors were identified by comparing the
674 cDNA sequences of *cis*-NATs against a database of miRNA hairpins downloaded from miRBase
675 (<http://www.mirbase.org>).

676

677 The presence of potential miRNA target mimic sites was determined using custom python functions
678 following the rules edicted in Wu et al. (2013), namely: (i) perfect nucleotide pairing was required
679 at the second to eighth positions of miRNA sequence, (ii) bulges were only permitted at the 5' end
680 ninth to 12th positions of miRNA sequence, and (iii) should be composed of only three nucleotides.
681 No more than 3 mismatches or G/U pairs were allowed in pairing regions (not considering the
682 bulge).

683

684 Analysis of siRNAs that could be generated by *cis*-NATs was essentially performed according to
685 the method described by Yuan et al. (2015) using the Arabidopsis small RNA dataset available on
686 GEO. Briefly, the small reads 18–28 nucleotides long were mapped to the TAIR10 reference
687 genome using bowtie. For each *cis*-NAT locus, the length and density in small RNAs was
688 calculated for overlapping and non-overlapping regions by dividing the number of mapped small
689 reads by the length of the region using custom scripts and the python library pysam.

690

691 The presence of transposable elements within *cis*-NAT transcripts was determined by comparing
692 the *cis*-NATs sequences against a database containing all transposable elements annotated in
693 TAIR10 using Blastn with a cutoff of $evalue=1e-12$ and percent identify > 50 .

694

695 **Quantification of TAIR10 and identified loci and identification of DEG**

696 For each experimental condition and biological replicate, the read count of TAIR10 as well as
697 identified loci was determined with HTSeq-count (mode Union) (Anders et al., 2015), and
698 normalized with DESeq2 (Love et al., 2014). A gene was considered differentially expressed
699 comparing two conditions if the $adj.pval < 0.1$ and the fold change > 2 or < 0.5 .

700

701 **Validation for DEG by RT-qPCR**

702 *A. thaliana* seedlings were grown in liquid cultures in the presence of a high or low concentration of
703 inorganic phosphate as described above in the “Plant materials” section. Total RNA was extracted
704 from whole seedlings with Trizol following manufacturer’s instructions. One microgram of RNA
705 was then used for reverse-transcription using the M-MLV Reverse Transcriptase (Promega) and
706 oligo d(T)₁₅ as primer using manufacturer's instructions. RT-qPCR analysis to measure mRNA
707 steady-state level was completed using SYBR select Master Mix (Applied Biosystems) with a
708 primer set specific of the gene of interest as well as a primers specific of *ACT2* gene used as
709 reference. Log₂ fold changes were calculated by the $\Delta\Delta Ct$ method.

710

711 **Determination of polysome association (PA) ratio**

712 To estimate the translation efficiency for each gene, the polysomes association (AP) ratio was
713 determined using Xtail package (Xiao et al., 2016), which calculates the ratio between read count
714 from polysomal RNA sample and total RNA sample. Genes with a Xtail $adj.pval < 0.1$ and at least a
715 30% increase or decrease of the AP ratio were considered differentially associated with polysomes.

716

717 **Identification *cis*-NATs influencing steady-state level or polysome association of cognate sense 718 mRNA**

719 The candidate regulatory *cis*-NATs were identified by pairwise comparisons between whole
720 seedlings grown under high- or low-Pi conditions, roots or shoots treated with phytohormones and
721 appropriate untreated controls, as well as between untreated root and shoot tissues, using a series of
722 criteria. Only the pairs coding gene / *cis*-NAT overlapping by at least 50 nucleotides and with a
723 normalized read count for both coding gene and *cis*-NAT > 20 were considered. A *cis*-NAT was
724 considered positively correlated to its cognate coding mRNA expression if both *cis*-NAT and
725 coding mRNA were either up-regulated or down-regulated (fold change > 2 and $adj.pval < 0.1$)

726 between the two conditions compared. It was considered negatively correlated if one partner was
727 up-regulated whereas the other was down-regulated (fold change > 2 and adj.pval < 0.1) between
728 the two conditions compared. To identify the putative translation regulatory *cis*-NATs, only the
729 pairs for which the coding gene was differentially translated with fold change > 1.3 and adj.pval <
730 0.1 between the two conditions compared, and with fold-change of mRNA steady-state level < 3
731 were kept. From these pairs, the *cis*-NATs had to be differentially expressed, with fold change > 2
732 and adj.pval < 0.1 and the ratio readcount *cis*-NAT / readcount coding gene had to be above 0.2, in
733 at least one condition. The *cis*-NATs up-regulated when their cognate mRNA was more associated
734 with polysomes were considered as putative translation enhancers, whereas *cis*-NATs up-regulated
735 when their cognate mRNA was less associated with polysomes were considered as putative
736 translation repressors.

737

738 Pearson correlation coefficient between mRNA and *cis*-NAT steady-state level was also calculated
739 across the 12 experimental conditions analyzed for each candidate pair with a positive or negative
740 correlation between *cis*-NAT and mRNA expression. Similarly, the correlation between PA ratio,
741 and *cis*-NAT steady-state level was also calculated across the 12 experimental conditions for each
742 translation regulator *cis*-NAT candidate. The candidate pairs with a correlation factor > 0.4 or < -
743 0.4 were considered as the most robust candidates.

744

745 **Creation and analysis of transgenic lines over-expressing putative translation regulatory *cis*-** 746 **NATs**

747 To create transgenic plants over-expressing the candidate translation regulator *cis*-NATs, the
748 genomic sequence encompassing the transcribed region was cloned into the vector pFAST-R02
749 (Shimada et al., 2010), in the correct orientation, to allow synthesis of the *cis*-NAT transcript under
750 the control of the cauliflower mosaic virus 35S promoter. The constructs were introduced into *A.*
751 *thaliana* by *Agrobacterium tumefaciens*-mediated transformation using floral dipping (Clough and
752 Bent, 1998). Transgenic lines over-expressing the different *cis*-NAT constructs or transformed with
753 empty vector were grown for 10 days on agar-solidified half-strength MS medium containing Basta
754 as a selection marker. Whole seedlings were crushed in liquid nitrogen and total RNA was extracted
755 using standard procedure.

756

757 To purify polysomes, 10-day-old seedlings were ground into powder in liquid nitrogen and 2
758 volumes of polysome extraction buffer were added. The mixture was incubated for 15 minutes on
759 ice, centrifuged at 16,000 *g* to pellet debris and 200 μ L of supernatant were loaded on top of 5 mL
760 sucrose gradients. After 75 min of centrifugation at 55,000 rpm in a SW55 rotor (Beckman) at 4°C,

761 the gradients were collected and split into 6 fractions. For each fraction, 500 μ L was transferred into
762 a new eppendorf tube and RNA was extracted with 1 mL of Trizol according to manufacturer's
763 instructions. An additional step of acetate ammonium precipitation with ethanol and washing was
764 added to remove remaining salt and phenol traces. For each sample, 300 ng of RNA was then used
765 for reverse transcription using the M-MLV Reverse Transcriptase (Promega) and oligo d(T)₁₅ as
766 primer using manufacturer's instructions. To analyze *WRKY45* mRNA, due to the full overlap
767 between *cis*-NAT and mRNA, the reverse transcription was performed in the same conditions but
768 using a mix of reverse primers specific to *WRKY45* and *ACT2* mRNA instead of oligo d(T)₁₅. RT-
769 qPCR analysis to quantify the relative amount of endogenous mRNA in each fraction was
770 performed with a primer set specific for the gene of interest as well as a primer specific for the
771 *ACT2* gene used as reference. The results are presented as relative proportion of endogenous mRNA
772 in each fraction of the gradient, as described in Faye et al. (2014). The average of 8 independent
773 biological replicates obtained with 2 independent transgenic lines is reported. To be able to quantify
774 in a more robust manner the changes in terms of polysome association, the sum of the proportions
775 of mRNA in fractions 1–3 and fractions 4–6 were calculated to compare the proportion of mRNA
776 not or poorly translated, e.g. free mRNA (fraction 1 and 2) or associated with monosomes (fraction
777 3), versus the proportion of mRNA efficiently translated, e.g. associated with low (fraction 4) or
778 high polysomes (fractions 5–6).

779

780 **Transient translation assays in Arabidopsis protoplasts**

781 Plasmids used for protoplast transformation were assembled using *Bsa*I-based Golden Gate cloning,
782 and the final constructs contained a recombination site for Gateway™ cloning. A Gateway™
783 destination vector, for cloning and expression of sense-coding genes, included a C-terminal in-
784 frame fusion with a foot-and-mouth disease virus (FMDV) 2A peptide, followed by fusion with
785 NanoLuc® luciferase (Nluc) (plasmid nLucFlucGW, GenBank MH552885). Additionally, an
786 independent expression cassette driving firefly luciferase (Fluc) was also included in this vector.
787 Another Gateway™ destination vector, for cloning and expression of antisense noncoding genes,
788 was produced without any fusion or additional expression cassette (plasmid RHIP1pGW, GenBank
789 MH552886). Both Gateway™ destination vectors expressed the cloned gene, sense or antisense,
790 under control of the same promoter (1.1 kbp genomic sequence upstream of AT4G26410) and
791 terminator (250 bp downstream of AT5G59720). Genomic sequences for sense-coding genes (from
792 5'UTR to last codon, without STOP) and antisense-noncoding genes were cloned via Gateway™
793 cloning into their corresponding vector.

794

795 Protoplasts were produced and transformed essentially as described by Yoo et al. (2007) with minor
796 modifications (see Supplemental Material and Methods). Protoplasts were harvested by
797 centrifugation at 6,000 g for 1 min, and resuspended in 1X Passive Lysis Buffer (Promega, E1941).
798 The lysate was cleared by centrifugation and used for luminescence quantification using Nano-
799 Glo® Dual-Luciferase® Reporter Assay System (Promega, N1610), according to the manufacture's
800 instructions. Luminescence values for Nluc fused to sense-coding gene were normalized against
801 Fluc to control for loading and transfection efficiency. Statistical significant differences (Student's
802 *t*-test, *p*-value < 0.05) in ratio Nluc:Fluc were used to assess the effect of antisense noncoding gene
803 co-expression.

804

805 **Quantification of NO production**

806 NO production was quantified in 10-day-old seedlings treated with spermidine following the
807 procedure described in Wimalakasera et al. (2011). Briefly, 5–6 seedlings were equilibrated in 3 mL
808 of MES buffer (30 mM MES, 0.1 mM CaCl₂, 1 mM KCl) for 2 h. Then 4,5-diaminofluorescein
809 diacetate and spermidine or DMSO was added to the medium. After 30 min incubation at 24°C
810 under light with shaking, 100 µL of medium was transferred to 96 well plate and fluorescence was
811 quantified. Eight independent biological replicates were analyzed and the fluorescence was
812 normalized by mg of fresh weight of spermidine-treated seedlings or untreated control.

813

814 **Accession numbers**

815 The data reported in this paper have been deposited in the Gene Expression Omnibus (GEO)
816 database, <https://www.ncbi.nlm.nih.gov/geo> (accession no. GSE116553). The processed data tables
817 (Supplemental Table S1 and S4) are included as additional files for this article. The sequence of
818 created plasmids used in this study has been submitted to GenBank, MH552885 and MH552886.

819

820 **Supplemental Data**

821 The following supplemental materials are available.

822 **Supplemental Figure S1.** Steady state mRNA expression level and association with polysomes in
823 response to treatment with phytohormones.

824 **Supplemental Figure S2.** GO terms enriched in the set of genes up-regulated in plants grown in
825 low Pi conditions or treated with various phytohormones.

826 **Supplemental Figure S3.** Analysis of the degree of overlap between independent studies analyzing
827 gene expression in response of low Pi or ABA treatment.

828 **Supplemental Figure S4.** GO terms enriched in the set of genes with changes in polysome
829 association.

830 **Supplemental Figure S5.** Steady state mRNA expression level and association with polysomes in
831 untreated roots compared to shoots.

832 **Supplemental Figure S6.** Evolutionary conservation of *cis*-NAT encoded peptides.

833 **Supplemental Figure S7.** Analysis of histone acetylation and nucleosome occupancy near the
834 transcription start site of *cis*-NATs.

835 **Supplemental Figure S8.** Analysis of the degree of overlap in *cis*-NATs identified in distinct
836 studies.

837 **Supplemental Figure S9.** Validation of differentially expressed genes by RT-qPCR.

838 **Supplemental Figure S10.** Proportion of the different types of orientation for the *cis*-NAT – sense
839 mRNA pairs.

840 **Supplemental Figure S11.** Analysis of *cis*-NAT-siRNAs.

841 **Supplemental Figure S12.** Quantification of the endogenous cognate mRNA in *cis*-NAT
842 overexpressing lines.

843 **Supplemental Figure S13.** Polysome profile.

844 **Supplemental Figure S14.** Levels of sense mRNA-NanoLuc luciferase (Nluc) fusion transcripts in
845 transiently transformed protoplasts.

846 **Supplemental Figure S15.** Quantification in NO production upon spermidine treatment.

847 **Supplemental Figure S16.** Organization of the *cis*-NAT:mRNA pair at AT1G03410 locus.

848 **Supplemental Table S1.** Summary of features associated with each transcript

849 **Supplemental Table S2.** Genes differentially expressed in various conditions

850 **Supplemental Table S3.** Number of mRNAs differentially associated with polysomes.

851 **Supplemental Table S4.** RNAseq and polysome profiling data relative to putative transcription or
852 translation regulatory *cis*-NATs.

853 **Supplemental Materials and Methods**

854

855

856

857

858 **Acknowledgements**

859 We thank the University of Lausanne Genomic Technology Facility for high-throughput sequencing
 860 support, the members of the Sinergia consortium, Jacques Rougemont (EPFL) and Bulak Arpat
 861 (SIB) for useful discussions, as well as Aidan Tay for help with statistical analysis. No conflict of
 862 interest declared.

863

864 **Tables**

865 **Table 1. Number of *cis*-NATs correlated with cognate gene steady-state mRNA expression or**
 866 **association with polysomes.** Number of mRNA / *cis*-NAT pairs with either a positive or negative
 867 correlation between *cis*-NAT and cognate gene steady-state mRNA expression (second and third
 868 columns), and number of pairs with positive or negative correlation between *cis*-NAT expression
 869 and cognate gene mRNA polysome association (PA) (fourth and fifth columns). The experimental
 870 conditions compared are indicated in the first column where root and shoot tissues are indicated
 871 with the prefix R and S, respectively, and untreated control conditions indicated with the suffix ctrl.
 872 The figures in brackets show the number of those pairs with a Pearson correlation coefficient > 0.4
 873 or < -0.4 across the 12 experimental correlations.

874

Treatment	Positive correlation <i>cis</i> -NAT / mRNA expression	Negative correlation <i>cis</i> -NAT / mRNA expression	Positive correlation <i>cis</i> -NAT expression / mRNA PA	Negative correlation <i>cis</i> -NAT expression / mRNA PA
Low / high Pi	40 (33)	10 (3)	4 (1)	1 (1)
RIAA / Rctrl	2 (2)	0	0	0
RABA / Rctrl	17 (13)	0	1 (0)	1 (0)
RMeJA / Rctrl	6 (4)	0	0	0
SABA / Sctrl	10 (7)	1 (0)	0	0
SMeJA / Sctrl	3 (3)	1 (0)	0	0
Rctrl / Sctrl	47 (41)	29 (24)	3 (2)	4 (2)
Total (unique)	107 (86)	41 (27)	8 (3)	6 (3)

875

876

877 **Figure legends**

878

879 **Figure 1. Steady state mRNA expression level and association with polysomes in response to**
 880 **growth of Arabidopsis under low-Pi conditions.** A, Relation between log₂-fold change of mRNA
 881 steady-state level (x axis) is plotted against the log₂-fold change in polysome association (y axis).
 882 Coding genes significantly up- or down-regulated at the mRNA steady-state level are colored in
 883 yellow and cyan, respectively, whereas mRNA significantly more or less associated with polysomes

884 are colored in red and blue, respectively. The genes not showing any statistical difference are
885 colored in grey. B, Same plot as A where genes associated with GO terms “Response to Pi
886 starvation”, “Cytosolic ribosome”, “Mitochondrial ribosome”, and “Chloroplastic ribosome” are
887 colored in pink, dark blue, light blue and green, respectively. C to E, Normalized RNA-seq
888 coverage plots for the *IPSI*, *RPS15AE* and *RPL34* genes. The two upper panels show the coverage
889 plots for total mRNA and polysomal RNA from high Pi samples and the two lower panels
890 correspond to low phosphate samples. The schematic exonic organization of each gene is
891 represented by red boxes and lines below the plots.

892 **Figure 2: Identification and characterization of *cis*-NATs.** A, Schematic diagram of the pipeline
893 used for *de novo cis*-NAT identification from the 12 different experimental conditions. B, Boxplot
894 comparing polysome association of *cis*-NATs predicted to be noncoding (green) or coding (pink),
895 ncRNA (cyan) and protein-coding genes (salmon) annotated in TAIR10 database. C and D, Plots
896 comparing transcript length (C) and RNA steady-state-level (D) of *cis*-NATs predicted to be
897 noncoding (green) or coding (pink), ncRNA (cyan) and protein-coding genes (salmon) annotated in
898 TAIR10 database. E, Boxplots comparing the nucleotide conservation across 20 angiosperm
899 genomes within exonic and intronic regions of the four categories of transcripts listed above.

900 **Figure 3: Correlations between expression of *cis*-NATs and changes in steady-state level or**
901 **poyslome association of the cognate sense mRNA.** A to D, Coverage plots showing the density of
902 RNA-seq reads per position at AT2G37580, AT1G68940, AT1G03410 and *CuAOI* loci. The red
903 and blue areas represent the density of reads mapping to the sense mRNA and *cis*-NATs,
904 respectively. For each experimental condition, the upper part corresponds to total RNA-seq reads
905 and the lower part to polysomal RNA-seq reads. The red and blue arrows below indicate the *cis*-
906 NAT-mRNA pair orientation. E to H, Correlation plots showing the steady-state level of the coding
907 mRNA (red dots) and *cis*-NAT (green dots) for AT2G37580 and AT1G68940 loci (E and F,
908 respectively) or the steady-state level of the *cis*-NAT (cyan dots) and the association with
909 polysomes of the cognate sense mRNA (purple dots) for AT1G03410 and *CuAOI* loci (G and H,
910 respectively). The Z-score of normalized read counts calculated from the 12 experimental
911 conditions is represented on the y-axis. Pearson correlation coefficients between the two variables
912 shown in each plot are indicated on top of the plots.

913 **Figure 4: Expression of putative translation repressor *cis*-NATs in transgenic *A. thaliana*.** A
914 and D, Coverage plots showing the density of RNA-seq reads per position for the *CuAOI* (A) and
915 AT1G54260 (D) loci, with the red and blue areas representing the sense mRNA and *cis*-NATs,
916 respectively. B and E, Polysome profiles showing the proportion of endogenous mRNA in each of

917 the six fractions of the sucrose gradient for transgenic lines over-expressing the *cis*-NAT (red)
918 versus that in control lines transformed with an empty vector (turquoise) for the *CuAOI* (B) and
919 AT1G54260 (E) sense mRNA-*cis*-NAT pair. C and F, Proportion of mRNA present in the first
920 three fractions (free RNA and monosomes) and in the last three fractions (polysomes) of the
921 gradient. Determinations were in transgenic lines over-expressing *cis*-NAT (red) and in control
922 lines transformed with an empty vector (turquoise) for the *CuAOI* (C) and AT1G54260 (F) sense
923 mRNA-*cis*-NAT pair. Data in B, C, E and F represent the average of 8 independent biological
924 replicates obtained with 2 independent transgenic lines. The error bars represent the confidence
925 intervals with $\alpha=0.05$. Asterisks indicate significant differences (Student's *t*-test with *p*-value
926 <0.05).

927 **Figure 5: Expression of putative translation activator *cis*-NATs in transgenic *A. thaliana*.** A
928 and D, Coverage plots showing the density of RNA-seq reads per position for the AT3G26240 (A)
929 and *WRKY45* (D) loci, with the red and blue areas representing the sense mRNA and *cis*-NATs,
930 respectively. B and E, Polysome profiles showing the proportion of endogenous mRNA in each of
931 the six fractions of the sucrose gradient for transgenic lines over-expressing the *cis*-NAT (red)
932 versus that in control lines transformed with an empty vector (turquoise) for the AT3G26240 (B)
933 and *WRKY45* (E) sense mRNA-*cis*-NAT pair. C and F, Proportion of mRNA present in the first
934 three fractions (free RNA and monosomes) and in the last three fractions (polysomes) of the
935 gradient, in transgenic lines over-expressing *cis*-NAT (red) and in control lines transformed with an
936 empty vector (turquoise) for the AT3G26240 (C) and *WRKY45* (F) sense mRNA-*cis*-NAT pair.
937 Data in B, C, E and F represent the average of 8 independent biological replicates obtained with 2
938 independent transgenic lines. The error bars represent the confidence intervals with $\alpha=0.05$.
939 Asterisks indicate significant differences (Student's *t*-test with *p*-value <0.05).

940
941 **Figure 6. Transient expression of putative translation repressor *cis*-NATs in protoplasts.**
942 Arabidopsis leaf protoplasts were co-transformed with a plasmid combining a sense mRNA-
943 NanoLuc luciferase (Nluc) fusion and a firefly luciferase (Fluc) along with various molar ratios of
944 an independent plasmid for expression of a *cis*-NAT. The ratio of Nluc over Fluc activity is plotted
945 for each combination of sense and *cis*-NAT plasmids. A, Co-expression of *CuAOI*-Nluc fusion with
946 its cognate *cis*-NAT. B, Co-expression of AT1G54260-Nluc with its cognate *cis*-NAT. C, Co-
947 expression of *CuAOI*-Nluc with the *cis*-NAT to AT1G54260. D, Co-expression of AT1G54260-
948 Nluc with the *cis*-NAT to *CuAOI*. Statistically significant differences (Student's *t*-test, *p*-value $<$
949 0.05; four biological replicates) between treatments are indicated by distinct letters above the boxes.
950

951 **Figure 7. Transient expression of putative translation activator *cis*-NATs in protoplasts.**
952 Arabidopsis leaf protoplasts were co-transformed with a plasmid combining a sense mRNA-
953 NanoLuc luciferase (Nluc) fusion and a firefly luciferase (Fluc) along with various molar ratios of
954 an independent plasmid for expression of a *cis*-NAT. The ratio of Nluc over Fluc activity is plotted
955 for each combination of sense and *cis*-NAT plasmids. A, Co-expression of AT3G26240-Nluc fusion
956 with its cognate *cis*-NAT. B, Co-expression of 2A6 (AT1G03410)-Nluc with its cognate *cis*-NAT.
957 C, Co-expression of *WRKY45* (AT3G01970)-Nluc with its cognate *cis*-NAT. D, Co-expression of
958 AT3G26240-Nluc with the *cis*-NAT to 2A6. E, Co-expression of 2A6-Nluc with the *cis*-NAT to
959 AT3G26240. Statistically significant differences (Student's *t*-test, *p*-value < 0.05; four biological
960 replicates) between treatments are indicated by distinct letters above the boxes.

961

962

963

964

965

966

967

Parsed Citations

Anders, S., Pyl, P. and Huber, W. (2015) HTSeq – A Python framework to work with high-throughput sequencing data. *Bioinformatics* 31: 166-169.

Pubmed: [Author and Title](#)

Google Scholar: [Author Only Title Only Author and Title](#)

Aspden, J.L., Eyre-Walker, Y.C., Philips, R.J., Amin, U., Muntaz, M.A.S., Brocard, M. and Couso, J.P. (2014) Extensive translation of small Open Reading Frames revealed by Poly-Ribo-Seq. *Elife* 3: e03528.

Pubmed: [Author and Title](#)

Google Scholar: [Author Only Title Only Author and Title](#)

Bardou, F., Ariel, F., Simpson, C.G., Romero-Barrios, N., Laporte, P., Balergue, S., Brown, J.W.S. and Crespi, M. (2014) Long noncoding RNA modulates alternative splicing regulators in *Arabidopsis*. *Dev. Cell* 30: 166-176.

Pubmed: [Author and Title](#)

Google Scholar: [Author Only Title Only Author and Title](#)

Bazin, J., Baerenfaller, K., Gosai, S.J., Gregory, B.D., Crespi, M. and Bailey-Serres, J. (2017) Global analysis of ribosome-associated noncoding RNAs unveils new modes of translational regulation. *Proc. Natl. Acad. Sci. USA* 114: E10018-E10027.

Pubmed: [Author and Title](#)

Google Scholar: [Author Only Title Only Author and Title](#)

Berardini, T.Z., Reiser, L., Li, D.H., Mezheritsky, Y., Muller, R., Strait, E. and Huala, E. (2015) The *Arabidopsis* information resource: Making and mining the "gold standard" annotated reference plant genome. *Genesis* 53: 474-485.

Pubmed: [Author and Title](#)

Google Scholar: [Author Only Title Only Author and Title](#)

Besson-Bard, A., Pugin, A. and Wendehenne, D. (2008) New insights into nitric oxide signaling in plants. *Annu. Rev. Plant Biol.* 59: 21-39.

Pubmed: [Author and Title](#)

Google Scholar: [Author Only Title Only Author and Title](#)

Bonasio, R. and Shiekhattar, R. (2014) Regulation of transcription by long noncoding RNAs. *Ann Rev Genet* 48: 433-455.

Pubmed: [Author and Title](#)

Google Scholar: [Author Only Title Only Author and Title](#)

Brockdorff, N., Ashworth, A., Kay, G.F., McCabe, V.M., Norris, D.P., Cooper, P.J., Swift, S. and Rastan, S. (1992) The product of the mouse *Xist* gene is a 15 kb inactive X-specific transcript containing no conserved ORF and located in the nucleus. *Cell* 71: 515-526.

Pubmed: [Author and Title](#)

Google Scholar: [Author Only Title Only Author and Title](#)

Carrieri, C., Cimatti, L., Biagioli, M., Beugnet, A., Zucchelli, S., Fedele, S., Pesce, E., Ferrer, I., Collavin, L., Santoro, C., et al. (2012) Long non-coding antisense RNA controls *Uchl1* translation through an embedded SINEB2 repeat. *Nature* 491: 454-457.

Pubmed: [Author and Title](#)

Google Scholar: [Author Only Title Only Author and Title](#)

Chekanova, J.A. (2015) Long non-coding RNAs and their functions in plants. *Curr. Opin. Plant Biol.* 27: 207-216.

Pubmed: [Author and Title](#)

Google Scholar: [Author Only Title Only Author and Title](#)

Cheng, C.Y., Krishnakumar, V., Chan, A.P., Thibaud-Nissen, F., Schobel, S. and Town, C.D. (2017) Araport11: a complete reannotation of the *Arabidopsis thaliana* reference genome. *Plant J.* 89: 789-804.

Pubmed: [Author and Title](#)

Google Scholar: [Author Only Title Only Author and Title](#)

Cho, J. and Paszkowski, J. (2017) Regulation of rice root development by a retrotransposon acting as a microRNA sponge. *Elife* 6: e30038.

Pubmed: [Author and Title](#)

Google Scholar: [Author Only Title Only Author and Title](#)

Clough, S.J. and Bent, A.F. (1998) Floral dip: a simplified method for *Agrobacterium*-mediated transformation of *Arabidopsis thaliana*. *Plant J.* 6: 735-743.

Pubmed: [Author and Title](#)

Google Scholar: [Author Only Title Only Author and Title](#)

Djebali, S., Davis, C.A., Merkel, A., Dobin, A., Lassmann, T., Mortazavi, A., Tanzer, A., Lagarde, J., Lin, W., Schlesinger, F., et al. (2012) Landscape of transcription in human cells. *Nature* 489: 101-108.

Pubmed: [Author and Title](#)

Google Scholar: [Author Only Title Only Author and Title](#)

Ebraldze, A.K., Guibal, F.C., Steidl, U., Zhang, P., Lee, S., Bartholdy, B., Jorda, M.A., Petkova, V., Rosenbauer, F., Huang, G., et al. (2008) PU.1 expression is modulated by the balance of functional sense and antisense RNAs regulated by a shared cis-regulatory element. *Genes Dev.* 22: 2085-2092.

Pubmed: [Author and Title](#)

Downloaded from on May 22, 2019 - Published by www.plantphysiol.org
Copyright © 2019 American Society of Plant Biologists. All rights reserved.

Google Scholar: [Author Only](#) [Title Only](#) [Author and Title](#)

Faghihi, M.A. and Wahlestedt, C. (2009) Regulatory roles of natural antisense transcripts. *Nat. Rev. Mol. Cell Biol.* 10: 637-643.

Pubmed: [Author and Title](#)

Google Scholar: [Author Only](#) [Title Only](#) [Author and Title](#)

Faghihi, M.A., Zhang, M., Huang, J., Modarresi, F., Van der Brug, M.P., Nalls, M.A., Cookson, M.R., St-Laurent, G., III and Wahlestedt, C. (2010) Evidence for natural antisense transcript-mediated inhibition of microRNA function. *Genome Biol.* 11: R56.

Pubmed: [Author and Title](#)

Google Scholar: [Author Only](#) [Title Only](#) [Author and Title](#)

Faye, M.D., Graber, T.E. and Holcik, M. (2014) Assessment of selective mRNA translation in mammalian cells by polysome profiling. *J Vis Exp* 28: e52295.

Pubmed: [Author and Title](#)

Google Scholar: [Author Only](#) [Title Only](#) [Author and Title](#)

Fedak, H., Palusinska, M., Krzyczmonik, K., Brzezniak, L., Yatusevich, R., Pietras, Z., Kaczanowski, S. and Swiezewski, S. (2016) Control of seed dormancy in *Arabidopsis* by a cis-acting noncoding antisense transcript. *Proc. Natl. Acad. Sci. USA* 113: E7846-E7855.

Pubmed: [Author and Title](#)

Google Scholar: [Author Only](#) [Title Only](#) [Author and Title](#)

Franco-Zorilla, J.M., Valli, A., Todesco, M., Mateos, I., Puga, M.I., Rubio-Somoza, I., Leyva, A., Weigel, D., Garcia, J.A. and Paz-Ares, J. (2007) Target mimicry provides a new mechanism for regulation of microRNA activity. *Nat. Genet.* 39: 1033-1037.

Pubmed: [Author and Title](#)

Google Scholar: [Author Only](#) [Title Only](#) [Author and Title](#)

Gao, W., Liu, W.W., Zhao, M. and Li, W.X. (2015) NERF encodes a RING E3 ligase important for drought resistance and enhances the expression of its antisense gene NFYA5 in *Arabidopsis*. *Nucleic Acids Res.* 43: 607-617.

Pubmed: [Author and Title](#)

Google Scholar: [Author Only](#) [Title Only](#) [Author and Title](#)

Gong, C.G. and Maquat, L.E. (2011) lncRNAs transactivate STAU1-mediated mRNA decay by duplexing with 3' UTRs via Alu elements. *Nature* 470: 284-288.

Pubmed: [Author and Title](#)

Google Scholar: [Author Only](#) [Title Only](#) [Author and Title](#)

Gupta, R.A., Shah, N., Wang, K.C., Kim, J., Horlings, H.M., Wong, D.J., Tsai, M.C., Hung, T., Argani, P., Rinn, J.L., et al. (2010) Long non-coding RNA HOTAIR reprograms chromatin state to promote cancer metastasis. *Nature* 464: 1071-1076.

Pubmed: [Author and Title](#)

Google Scholar: [Author Only](#) [Title Only](#) [Author and Title](#)

Hart-Smith, G., Reis, R.S., Waterhouse, P.M. and Wilkins, M.R. (2017) Improved Quantitative Plant Proteomics via the Combination of Targeted and Untargeted Data Acquisition. *Front Plant Sci* 8:

Pubmed: [Author and Title](#)

Google Scholar: [Author Only](#) [Title Only](#) [Author and Title](#)

Held, M.A., Penning, B., Brandt, A.S., Kessans, S.A., Yong, W.D., Scofield, S.R. and Carpita, N.C. (2008) Small-interfering RNAs from natural antisense transcripts derived from a cellulose synthase gene modulate cell wall biosynthesis in barley. *Proc. Natl. Acad. Sci. USA* 105: 20534-20539.

Pubmed: [Author and Title](#)

Google Scholar: [Author Only](#) [Title Only](#) [Author and Title](#)

Heo, J.B. and Sung, S. (2011) Vernalization-mediated epigenetic silencing by a long intronic noncoding RNA. *Science* 331: 76-79.

Pubmed: [Author and Title](#)

Google Scholar: [Author Only](#) [Title Only](#) [Author and Title](#)

Hergeth, S.P. and Schneider, R. (2015) The H1 linker histones: multifunctional proteins beyond the nucleosomal core particle. *EMBO Rep.* 16: 1439-1453.

Pubmed: [Author and Title](#)

Google Scholar: [Author Only](#) [Title Only](#) [Author and Title](#)

Hsu, P.Y., Calviello, L., Wu, H.-Y.L., Li, F.-W., Rothfels, C.J., Ohler, U. and Benfey, P.N. (2016) Super-resolution ribosome profiling reveals unannotated translation events in *Arabidopsis*. *Proc. Natl. Acad. Sci. USA* 113: E7126-E7135.

Pubmed: [Author and Title](#)

Google Scholar: [Author Only](#) [Title Only](#) [Author and Title](#)

Hu, G.Z., Lou, Z.K. and Gupta, M. (2014) The long non-coding RNA GAS5 cooperates with the eukaryotic translation initiation factor 4E to regulate c-Myc translation. *Plos One* 9: e107016.

Pubmed: [Author and Title](#)

Google Scholar: [Author Only](#) [Title Only](#) [Author and Title](#)

Hupaló, D. and Kern, A.D. (2013) Conservation and functional element discovery in 20 angiosperm plant genomes. *Mol. Biol. Evol.* 30: 1729-1744.

Pubmed: [Author and Title](#)

Google Scholar: [Author Only](#) [Title Only](#) [Author and Title](#)

- Jabnourne, M., Secco, D., Lecampion, C., Robaglia, C., Shu, Q. and Poirier, Y. (2013) A rice cis-natural antisense RNA acts as a translational enhancer for its cognate mRNA and contributes to phosphate homeostasis and plant fitness. *Plant Cell* 25: 4166-4182.
Pubmed: [Author and Title](#)
Google Scholar: [Author Only](#) [Title Only](#) [Author and Title](#)
- Jegu, T., Veluchamy, A., Ramirez-Prado, J.S., Rizzi-Paillet, C., Perez, M., Lhomme, A., Latrasse, D., Coleno, E., Vicaire, S., Legras, S., et al. (2017) The Arabidopsis SWI/SNF protein BAF60 mediates seedling growth control by modulating DNA accessibility. *Genome Biol.* 18:
Pubmed: [Author and Title](#)
Google Scholar: [Author Only](#) [Title Only](#) [Author and Title](#)
- Ji, Z., Song, R., Regev, A. and Struhl, K. (2015) Many lncRNAs, 5' UTRs, and pseudogenes are translated and some are likely to express functional proteins. *Elife* 4: e08890.
Pubmed: [Author and Title](#)
Google Scholar: [Author Only](#) [Title Only](#) [Author and Title](#)
- Jin, J., Liu, J., Wang, H., Wong, L. and Chua, N.-H. (2013) PLncDB: plant long non-coding RNA database. *Bioinformatics* 29: 1068-1071.
Pubmed: [Author and Title](#)
Google Scholar: [Author Only](#) [Title Only](#) [Author and Title](#)
- Juntawong, P., Girke, T., Bazin, J. and Bailey-Serres, J. (2014) Translational dynamics revealed by genome-wide profiling of ribosome footprints in Arabidopsis. *Proc. Natl. Acad. Sci. USA* 111: E203-E212.
Pubmed: [Author and Title](#)
Google Scholar: [Author Only](#) [Title Only](#) [Author and Title](#)
- Khorkova, O., Myers, A.J., Hsiao, J. and Wahlestedt, C. (2014) Natural antisense transcripts. *Hum. Mol. Genet.* 23: R54-R63.
Pubmed: [Author and Title](#)
Google Scholar: [Author Only](#) [Title Only](#) [Author and Title](#)
- Kim, D., Landmead, B. and Salzberg, S.L. (2015) HISAT: a fast spliced aligner with low memory requirements. *Nat. Methods* 12: 357-U121.
Pubmed: [Author and Title](#)
Google Scholar: [Author Only](#) [Title Only](#) [Author and Title](#)
- Kino, T., Hurt, D.E., Ichijo, T., Nader, N. and Chrousos, G.P. (2010) Noncoding RNA Gas5 is a growth arrest- and starvation-associated repressor of the glucocorticoid receptor. *Science Signal* 3: ra8.
Pubmed: [Author and Title](#)
Google Scholar: [Author Only](#) [Title Only](#) [Author and Title](#)
- Kotlinski, M., Knizewski, L., Muszewska, A., Rutowicz, K., Lirski, M., Schmidt, A., Baroux, C., Ginalski, K. and Jerzmanowski, A. (2017) Phylogeny-based systematization of Arabidopsis proteins with histone H1 globular domain. *Plant Physiol.* 174: 27-34.
Pubmed: [Author and Title](#)
Google Scholar: [Author Only](#) [Title Only](#) [Author and Title](#)
- Lapidot, M. and Pilpel, Y. (2006) Genome-wide natural antisense transcription: coupling its regulation to its different regulatory mechanisms. *EMBO Rep.* 7: 1216-1222.
Pubmed: [Author and Title](#)
Google Scholar: [Author Only](#) [Title Only](#) [Author and Title](#)
- Laubinger, S., Sachsenberg, T., Zeller, G., Busch, W., Lohmann, J.U., Raescht, G. and Weigel, D. (2008) Dual roles of the nuclear cap-binding complex and SERRATE in pre-mRNA splicing and microRNA processing in Arabidopsis thaliana. *Proc. Natl. Acad. Sci. USA* 105: 8795-8800.
Pubmed: [Author and Title](#)
Google Scholar: [Author Only](#) [Title Only](#) [Author and Title](#)
- Liu, F., Marquardt, S., Lister, C., Swiezewski, S. and Dean, C. (2010) Targeted 3' processing of antisense transcripts triggers Arabidopsis FLC chromatin silencing. *Science* 327: 94-97.
Pubmed: [Author and Title](#)
Google Scholar: [Author Only](#) [Title Only](#) [Author and Title](#)
- Liu, J., Wang, H. and Chua, N.-H. (2015) Long noncoding RNA transcriptome of plants. *Plant Biotechnol. J.* 13: 319-328.
Pubmed: [Author and Title](#)
Google Scholar: [Author Only](#) [Title Only](#) [Author and Title](#)
- Love, M., Huber, W. and Anders, S. (2014) Moderated estimation of fold change and dispersion for RNA-seq data with DESeq2. *Genome Biol.* 15: 550.
Pubmed: [Author and Title](#)
Google Scholar: [Author Only](#) [Title Only](#) [Author and Title](#)
- Mondal, T., Rasmussen, M., Pandey, G.K., Isaksson, A. and Kanduri, C. (2010) Characterization of the RNA content of chromatin. *Genome Res.* 20: 899-907.
Pubmed: [Author and Title](#)
Google Scholar: [Author Only](#) [Title Only](#) [Author and Title](#)
- Mustroph, A., Zanetti, M.E., Jang, C.-H., Holtan, H.F., Repetti, P.P., Galbraith, D.W., Girke, T. and Bailey-Serres, J. (2009) Profiling

translatomes of discrete cell populations resolves altered cellular priorities during hypoxia in Arabidopsis. Proc. Natl. Acad. Sci. USA 106: 18843-18848.

Pubmed: [Author and Title](#)

Google Scholar: [Author Only Title Only Author and Title](#)

Rangwala, S.H. and Richards, E.J. (2010) The structure, organization and radiation of Sadhu non-long terminal repeat retroelements in Arabidopsis species. Mobile DNA 1: 10.

Pubmed: [Author and Title](#)

Google Scholar: [Author Only Title Only Author and Title](#)

Ransohoff, J.D., Wei, Y. and Khavari, P.A. (2018) The functions and unique features of long intergenic non-coding RNA. Nature Rev Mol Cell Biol 19: 143-157.

Pubmed: [Author and Title](#)

Google Scholar: [Author Only Title Only Author and Title](#)

Rinn, J.L. and Chang, H.Y. (2012) Genome regulation by long noncoding RNAs. Annu. Rev. Biochem. 81: 145-166.

Pubmed: [Author and Title](#)

Google Scholar: [Author Only Title Only Author and Title](#)

Ron, M., Saez, M.A., Williams, L.E., Fletcher, J.C. and McCormick, S. (2010) Proper regulation of a sperm-specific cis-nat-siRNA is essential for double fertilization in Arabidopsis. Genes Dev. 24: 1010-1021.

Pubmed: [Author and Title](#)

Google Scholar: [Author Only Title Only Author and Title](#)

Rosa, S., Duncan, S. and Dean, C. (2016) Mutually exclusive sense-antisense transcription at FLC facilitates environmentally induced gene repression. Nat Commun 7: 13031.

Pubmed: [Author and Title](#)

Google Scholar: [Author Only Title Only Author and Title](#)

Schein, A., Zucchelli, S., Kauppinen, S., Gustincich, S. and Carninci, P. (2016) Identification of antisense long noncoding RNAs that function as SINEUPs in human cells. Scientific Reports 6: 33605.

Pubmed: [Author and Title](#)

Google Scholar: [Author Only Title Only Author and Title](#)

Schmitz, K.M., Mayer, C., Postepska, A. and Grummt, I. (2010) Interaction of noncoding RNA with the rDNA promoter mediates recruitment of DNMT3b and silencing of rRNA genes. Genes Dev. 24: 2264-2269.

Pubmed: [Author and Title](#)

Google Scholar: [Author Only Title Only Author and Title](#)

Seo, J.S., Sun, H.X., Park, B.S., Huang, C.H., Yeh, S.D., Jung, C. and Chua, N.H. (2017) ELF18-INDUCED LONG-NONCODING RNA associates with Mediator to enhance expression of innate immune response genes in Arabidopsis. Plant Cell 29: 1024-1038.

Pubmed: [Author and Title](#)

Google Scholar: [Author Only Title Only Author and Title](#)

Shimada, T.L., Shimada, T. and Hara-Nishimura, I. (2010) A rapid and non-destructive screenable marker, FAST, for identifying transformed seeds of Arabidopsis thaliana. Plant J. 61: 519-528.

Pubmed: [Author and Title](#)

Google Scholar: [Author Only Title Only Author and Title](#)

Song, L., Huang, S.S.C., Wise, A., Castanon, R., Nery, J.R., Chen, H.M., Watanabe, M., Thomas, J., Bar-Joseph, Z. and Ecker, J.R. (2016) A transcription factor hierarchy defines an environmental stress response network. Science 354: aag1550.

Pubmed: [Author and Title](#)

Google Scholar: [Author Only Title Only Author and Title](#)

Sun, H., Bi, Y., Tao, J., Huang, S., Hou, M., Xue, R., Liang, Z., Gu, P., Yoneyama, K., Xie, X., et al. (2016) Strigolactones are required for nitric oxide to induce root elongation in response to nitrogen and phosphate deficiencies in rice. Plant Cell Environ. 39: 1473-1484.

Pubmed: [Author and Title](#)

Google Scholar: [Author Only Title Only Author and Title](#)

Tran, N.T., Su, H.R., Khodadadi-Jamayran, A., Lin, S., Zhang, L., Zhou, D.W., Pawlik, K.M., Townes, T.M., Chen, Y.B., Mulloy, J.C., et al. (2016) The AS-RBM15 lncRNA enhances RBM15 protein translation during megakaryocyte differentiation. EMBO Rep. 17: 887-900.

Pubmed: [Author and Title](#)

Google Scholar: [Author Only Title Only Author and Title](#)

Trapnell, C., Williams, B.A., Pertea, G., Mortazavi, A., Kwan, G., van Baren, M.J., Salzberg, S.L., Wold, B.J. and Pachter, L. (2010) Transcript assembly and quantification by RNA-Seq reveals unannotated transcripts and isoform switching during cell differentiation. Nat. Biotechnol. 28: 511-515.

Pubmed: [Author and Title](#)

Google Scholar: [Author Only Title Only Author and Title](#)

Tripathi, V., Ellis, J.D., Shen, Z., Song, D.Y., Pan, Q., Watt, A.T., Freier, S.M., Bennett, C.F., Sharma, A., Bubulya, P.A., et al. (2010) The nuclear-retained noncoding RNA MALAT1 regulates alternative splicing by modulating SR splicing factor phosphorylation. Mol. Cell 39: 925-938.

Pubmed: [Author and Title](#)

Google Scholar: [Author Only Title Only Author and Title](#)

- Wang, H., Chung, P.J., Liu, J., Jang, I.-C., Kean, M.J., Xu, J. and Chua, N.-H. (2014) Genome-wide identification of long noncoding natural antisense transcripts and their responses to light in *Arabidopsis*. *Genome Res.* 24: 444-453.
Pubmed: [Author and Title](#)
Google Scholar: [Author Only Title Only Author and Title](#)
- Wang, X.J., Gaasterland, T. and Chua, N.H. (2005) Genome-wide prediction and identification of cis-natural antisense transcripts in *Arabidopsis thaliana*. *Genome Biol.* 6: R30.
Pubmed: [Author and Title](#)
Google Scholar: [Author Only Title Only Author and Title](#)
- Wang, Y., Xu, Z., Jiang, J., Xu, C., Kang, J., Xiao, L., Wu, M., Xiong, J., Guo, X. and Liu, H. (2013) Endogenous miRNA sponge lincRNA-RoR regulates Oct4, Nanog, and Sox2 in human embryonic stem cell self-renewal. *Dev. Cell* 25: 69-80.
Pubmed: [Author and Title](#)
Google Scholar: [Author Only Title Only Author and Title](#)
- Weiner, A.M. (2002) SINEs and LINEs: the art of biting the hand that feeds you. *Curr. Opin. Cell Biol.* 14: 343-350.
Pubmed: [Author and Title](#)
Google Scholar: [Author Only Title Only Author and Title](#)
- Wimalasekera, R., Villar, C., Begum, T. and Scherer, G.F.E. (2011) COPPER AMINE OXIDASE1 (CuAO1) of *Arabidopsis thaliana* contributes to abscisic acid- and polyamine-induced nitric oxide biosynthesis and abscisic acid signal transduction. *Mol Plant* 4: 663-678.
Pubmed: [Author and Title](#)
Google Scholar: [Author Only Title Only Author and Title](#)
- Wu, H.-J., Wang, Z.-M., Wang, M. and Wang, X.-J. (2013) Widespread long noncoding RNAs as endogenous target mimics for microRNAs in plants. *Plant Physiol.* 161: 1875-1884.
Pubmed: [Author and Title](#)
Google Scholar: [Author Only Title Only Author and Title](#)
- Wucher, V., Legeai, F., Hedan, B., Rizk, G., Lagoutte, L., Leeb, T., Jagannathan, V., Cadieu, E., David, A., Lohi, H., et al. (2017) FEELnc: a tool for long non-coding RNA annotation and its application to the dog transcriptome. *Nucleic Acids Res.* 45: e57.
Pubmed: [Author and Title](#)
Google Scholar: [Author Only Title Only Author and Title](#)
- Xiao, Z.T., Zou, Q., Liu, Y. and Yang, X.R. (2016) Genome-wide assessment of differential translations with ribosome profiling data. *Nat Comm* 7: 11194.
Pubmed: [Author and Title](#)
Google Scholar: [Author Only Title Only Author and Title](#)
- Yoo, S.-D., Cho, Y.-H. and Sheen, J. (2007) *Arabidopsis* mesophyll protoplasts: a versatile cell system for transient gene expression analysis. *Nat Protoc* 2: 1565-1572.
Pubmed: [Author and Title](#)
Google Scholar: [Author Only Title Only Author and Title](#)
- Yoon, J.H., Abdelmohsen, K., Srikantan, S., Yang, X.L., Martindale, J.L., De, S., Huarte, M., Zhan, M., Becker, K.G. and Gorospe, M. (2012) LincRNA-p21 suppresses target mRNA translation. *Mol. Cell* 47: 648-655.
Pubmed: [Author and Title](#)
Google Scholar: [Author Only Title Only Author and Title](#)
- Yuan, C.H., Wang, J.J., Harrison, A.P., Meng, X.W., Chen, D.J. and Chen, M. (2015) Genome-wide view of natural antisense transcripts in *Arabidopsis thaliana*. *DNA Res.* 22: 233-243.
Pubmed: [Author and Title](#)
Google Scholar: [Author Only Title Only Author and Title](#)
- Yuan, J.P., Zhang, Y., Dong, J.S., Sun, Y.Z., Lim, B.L., Liu, D. and Lu, Z.J. (2016) Systematic characterization of novel lincRNAs responding to phosphate starvation in *Arabidopsis thaliana*. *BMC Genom* 17: 655.
Pubmed: [Author and Title](#)
Google Scholar: [Author Only Title Only Author and Title](#)
- Zhang, X.-N., Shi, Y., Powers, J.J., Gowda, N.B., Zhang, C., Ibrahim, H.M.M., Ball, H.B., Chen, S.L., Lu, H. and Mount, S.M. (2017) Transcriptome analyses reveal SR45 to be a neutral splicing regulator and a suppressor of innate immunity in *Arabidopsis thaliana*. *BMC Genom* 18: 772.
Pubmed: [Author and Title](#)
Google Scholar: [Author Only Title Only Author and Title](#)
- Zhou, X.F., Sunkar, R., Jin, H.L., Zhu, J.K. and Zhang, W.X. (2009) Genome-wide identification and analysis of small RNAs originated from natural antisense transcripts in *Oryza sativa*. *Genome Res.* 19: 70-78.
Pubmed: [Author and Title](#)
Google Scholar: [Author Only Title Only Author and Title](#)
- Zhou, Y., Hartwig, B., James, G.V., Schneeberger, K. and Turck, F. (2016) Complementary activities of TELOMERE REPEAT BINDING proteins and polycomb group complexes in transcriptional regulation of target genes. *Plant Cell* 28: 87-101.

Pubmed: [Author and Title](#)

Google Scholar: [Author Only](#) [Title Only](#) [Author and Title](#)